National Library of Canada
Bibliothèque nationale du Canada

Canadian Theses Service
Service des thèses canadiennes

Ottawa, Canada
K1A 0N4

NOTICE

The quality of this microform is heavily dependent upon the quality of the original thesis submitted for microfilming. Every effort has been made to ensure the highest quality of reproduction possible.

If pages are missing, contact the university which granted the degree.

Some pages may have indistinct print especially if the original pages were typed with a poor typewriter ribbon or if the university sent us an inferior photocopy.

Reproduction in full or in part of this microform is governed by the Canadian Copyright Act, R.S.C. 1970, c. C-30, and subsequent amendments.

AVIS

La qualité de cette microforme dépend grandement de la qualité de la thèse soumise au microfilmage. Nous avons tout fait pour assurer une qualité supérieure de reproduction

S'il manque des pages, veuillez communiquer avec l'université qui a conféré le grade.

La qualité d'impression de certaines pages peut laisser à désirer, surtout si les pages originales ont été dactylographiées à l'aide d'un ruban usé ou si l'université nous a fait parvenir une photocopie de qualité inférieure

La reproduction, même partielle, de cette microforme est soumise à la Loi canadienne sur le droit d'auteur, SRC 1970, c. C-30, et ses amendements subséquents

Canada

National Library of Canada
Bibliothèque nationale du Canada

Canadian Theses Service
Service des thèses canadiennes

Ottawa, Canada
K1A 0N4

The author has granted an irrevocable non-exclusive licence allowing the National Library of Canada to reproduce, loan, distribute or sell copies of his/her thesis by any means and in any form or format, making this thesis available to interested persons.

The author retains ownership of the copyright in his/her thesis. Neither the thesis nor substantial extracts from it may be printed or otherwise reproduced without his/her permission.

L'auteur a accordé une licence irrévocable et non exclusive permettant à la Bibliothèque nationale du Canada de reproduire, prêter, distribuer ou vendre des copies de sa thèse de quelque manière et sous quelque forme que ce soit pour mettre des exemplaires de cette thèse à la disposition des personnes intéressées.

L'auteur conserve la propriété du droit d'auteur qui protège sa thèse. Ni la thèse ni des extraits substantiels de celle-ci ne doivent être imprimés ou autrement reproduits sans son autorisation.

ISBN 0-315-56125-4

Canada

Active Input Current Waveshaping Techniques for Single-Phase Front-End Diode-Rectifiers

Mehrdad Kazerani

A Thesis

in

The Department

of

Electrical and Computer Engineering

Presented in Partial Fulfillment of the Requirements
for the Degree of Master of Engineering at
Concordia University
Montreal, Quebec, Canada

March 1990

©Mehrdad Kazerani, 1990

ABSTRACT

ACTIVE INPUT CURRENT WAVESHAPING TECHNIQUES FOR SINGLE-PHASE FRONT-END DIODE-RECTIFIERS

Mehrdad Kazerani

Front-end diode-rectifiers feeding into a capacitive filter, exhibit a very low power factor and inject current harmonics of large amplitudes into the grid. The problem is worse when the load fed on the DC bus is nonlinear, which is often the case. With the increasing demand for more efficient utilization of the utility source and line transmission capacity, input power factor conditioning is gradually becoming a "must" for medium to high power level electronic equipment fed from a DC bus comprised of the typical diode rectifier-DC capacitor combination. Active input current waveshaping techniques are employed for such purposes, among which the hysteresis method is the most widely used. This technique has a very fast response and a simple implementation, but results in varying switching frequency.

Novel active input current waveshaping techniques for single-phase front-end diode-rectifiers are investigated in this thesis. One class of methods based on Error Triangulation, features fixed switching frequency (an advantage over the hysteresis technique), fast response, and controllable input current ripple. By introducing an integral term in the current

regulator, the shape of the input current is further improved.

The second class of methods proposed is based on a predictive approach to input current waveshaping. This method has the advantages of the previous method and is also microprocessor-implementable. A simplified version of the above technique eliminates the need for the input current sensing, but exhibits higher parameter sensitivity.

For the proposed methods, the principles of operation and the design procedures for the power circuit and the control unit are derived. Theoretical predictions are verified by the simulation and experimental results.

ACKNOWLEDGEMENTS

I wish to express my gratitude to Dr. P. D. Ziogas and Dr. G. Joos for their valuable advice and support during the course of this study.

I like to thank all my friends and research colleagues in Power Lab for helping me any time I asked for it. Thanks to Danny Juras for his laboratory assistance.

Special gratitude to my wife for her understanding and encouragement during the preparation of this thesis.

TABLE OF CONTENTS

CHAPTER 3 ERROR TRIANGULATION METHOD

LIST OF FIGURES

LIST OF TABLES

LIST OF ACRONYMS

BBH	bang-bang hysteresis
DPF	displacement power factor
EMI	electromagnetic interference
mH	mili Henry
MOSFET	metal oxide semiconductor field effect transistor
P	proportional
P.F.	power factor
PI	proportional integral
PWM	pulse width modulation
rms	root mean square
SW	switch
THD	total harmonic distortion
kVA	kilo Volt Amperes
μF	micro Farad
p.u.	per unit

LIST OF PRINCIPAL SYMBOLS

a	ratio of DC component of output voltage to peak value of AC input voltage
A_{min}	minimum amplitude of the triangular waveform
C	capacitor, capacitance
C_B	base value for capacitance
C_f	capacitance of PI-controller feedback capacitor
d	average ON-duty ratio of the switch in one switching period
$\overline{D}$	average ON-duty ratio of the switch in a half cycle of the AC input voltage
d'	average OFF-duty ratio of the switch in one switching period
E	output of voltage controller at operating point
e	output of voltage controller
$\hat{e}$	small perturbation in the output of voltage controller
f_B	base value for frequency
f_b	break frequency of the LC filter
f_{IN}, f_{line}	frequency of the AC input voltage
f_{sw}	switching frequency
$f_{sw,ave}$	average switching frequency in a half cycle of the AC input voltage
$G_{AC}(s)$	AC gain of the output filter
$G_{DC}(s)$	DC gain of the output filter
I_B	base value for the current
i_C	capacitor current

i_D	boost diode current
$i_{D,ave}, \bar{I}_D$	average of the boost diode current in a half cycle of the AC input voltage
$I_1, I_{1,rms}$	rms value of the fundamental component of the current
I_h	rms value of the h^{th} harmonic of the current
i_L	boost inductor current
$\bar{I}_L$	average of inductor current in a half cycle of the AC input voltage
$i_{L,fbk}$	inductor current feedback signal
$i_{L,ref}, i_r$	inductor current reference signal
$I_{n,rms}$	rms value of the n^{th} harmonic of the current
$I_{ns,rms}$	rms value of the current harmonic at the switching frequency
i_{rD}	rectifier diode current
$I_{ref,rms}$	rms value of the current reference
$I_{1r,rms}$	rms value of the fundamental component of the ripple current
I_s	current source
i_s	current through the AC source
$\lvert i_s \rvert$	full-wave rectified source current
$i_{s,peak}, I_m$	peak value of the current through the AC source
i_{sw}	switch current
I_t	rms value of the total current
k	$K_1 * K_2$
K_1	ratio of i_L to $i_{L,ref}$
K_2	ratio of $i_{L,ref}$ to $\lvert v_s \rvert$
K_I	integral coefficient of PI-controller
K_P	proportional coefficient of PI-controller

L	inductor, inductance
L_B	base value for inductance
m	slope
m_{ON}	slope of the inductor current during the ON-period of the switch
m_{OFF}	slope of the inductor current during the OFF-period of the switch
P	a factor equal to +1 in the positive half cycle of the AC input voltage and equal to -1 in the negative half cycle of the AC input voltage
P_B	base value for power
P_o	output power
R	resistance
r	ratio of peak-to-peak value of output voltage ripple to the DC component of the output voltage
R_f	resistance of PI-controller feedback resistor
R_i	resistance of PI-controller input resistor
R_L	load resistance
$T_F(s)$	transfer function of the LC filter
t_{ON}	ON-period of the switch
t_{OFF}	OFF-period of the switch
$T_{PI}(s)$	transfer function of PI-controller
T_{sw}	switching period
V_B	base value for voltage
v_C	capacitor voltage
$V_i(s)$	input voltage of PI-controller
v_L	inductor voltage
V_1	rms value of the fundamental component of the voltage

V_o	DC component of output voltage
v_o	output voltage
$\overline{V}_o$	output voltage at operating point
$\hat{V}_o$	small perturbation in the output voltage
$V_o(s)$	output voltage of PI-controller
v_{or}	ripple component of the output voltage
$v_{or,peak}$	peak-to-peak value of v_{or}
v_{rev}	diode reverse voltage
v_s	AC source voltage
$\lvert v_s \rvert$	full-wave rectified AC source voltage
$v_{s,peak}, V_m$	peak value of the AC input voltage
v_{sw}	voltage across the switch during its OFF-period
V_t	rms value of the total voltage
W_{peak}	minimum value of the maximum stored energy in the power processor
Z_B	base value for impedance
ΔI	hysteresis window width, peak-to-peak value of current ripple
ζ	damping ratio of the LC filter
ϕ_1	angle between the fundamental components of voltage and current
ω	angular frequency in radians per second (rad/s)
ω_n	natural angular frequency of the LC filter

CHAPTER 1

INTRODUCTION

1.1 Introduction

From the point of view of the power system, a high power factor load results in high efficiency in electric power consumption and better utilization of utility source and line capacity [1]. Maximizing the power factor is therefore becoming a very important issue since, sources and supplies of electric power are limited (even though the limit has not been reached yet), and construction of generating capacity is expensive. This calls for more efficient operation of the existing sources and installations of utilities.

Power factor is defined, in its most general form, as the ratio of the real power to the apparent power:

$$P.F. = \frac{\text{Real Power}}{\text{Apparent Power}} = \frac{\sum_{n=1}^{\infty} V_n I_n \cos \phi_n}{V_t I_t} \qquad (1.1)$$

where V_n, I_n, V_t, I_t, and ϕ_n are the rms values of the $n^{th.}$ harmonics of the voltage and current, the rms values of the total voltage and current, and the angle between the $n^{th.}$ components of voltage and current respectively.

Assuming the line voltage to be a distortion-free sinusoid, Eqn. 1.1 reduces to

$$P.F. = \frac{I_1}{I_t} \cos\phi_1 = \frac{I_1}{I_t} DPF \qquad (1.2)$$

where DPF is the displacement power factor.

It results from Eqn. 1.2 that power factor degradation is caused by current waveform distortion and/or phase displacement of the fundamental component of the current with respect to the voltage. In the case where $I_1=I_t$ (i.e., no distortion in the input current), and DPF<1, only the component of current in phase with the input voltage contributes to the useful power delivered to the load, but the total rms current determines the amount of line losses. Also, when the input current waveform is distorted, harmonic currents will be injected in the utility line. These injected harmonics contribute to the total rms current in the line which determines the amount of losses, but do not contribute to the useful power delivered to the load. As seen, both factors causing P.F. degradation, result in loss of electrical efficiency and poorer utilization of the utility source and line capacity.

Harmonic injection into the AC line, in presence of the utility source and line impedances, causes distortion in the voltage at the common coupling point of the harmonic generating load and other loads. Furthermore, the harmonic currents can cause additional heating and overvoltages (due to resonance conditions) in the utility's transmission and distribution equipment, errors in metering and protection, and have a negative impact on the communication and control signals [1].

Input power factor conditioning is gradually becoming a mandatory requirement for medium to high power level electronic equipment fed from a DC bus comprised of the typical diode rectifier - DC capacitor combination (Fig.

1.1), [2]-[14].

Even for the simplest case where the load is purely resistive, because of the presence of the DC filter capacitor (C_f) at the rectifier output, (Fig. 1.1), the current drawn from the utility, by the circuit of Fig. 1.1, is highly distorted and contains harmonic components of large magnitudes (Table 1.1). Nonlinearities in real loads, especially static converter and switched-mode converter loads, increase the input current harmonics. This results in a very poor power factor.

A high power factor (very close to unity) is obtained by forcing I_1 and I_t (Eqn. 1.2) to be very close to each other, and making DPF very close to 1. This means that power factor can be improved by shaping the input current to be a sinusoid, just as the input voltage.

1.2 Input Power Factor Improvement through Input Current Waveshaping

There are two different approaches to obtain a higher power factor at the input of diode-rectifier circuits [1],[2]. One is filtering harmonic currents at the interface with the utility. Passive input current waveshaping methods use this approach. Passive methods have the obvious advantage of simplicity and reliability, but they can not keep the current waveform independent of the load i.e., the input power factor can be optimized for a narrow range of operating points [15]. The second approach is preventing harmonic currents from being generated (or minimizing them). This approach is taken in active input current waveshaping techniques. Active methods provide possibility of using advanced control methods and can make the current waveform independent of the load.

The common practice in active methods is to place a switched-mode DC/DC

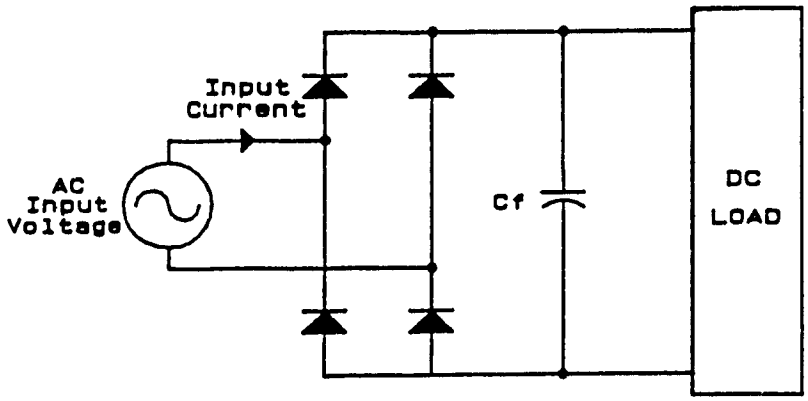

Fig. 1.1 A simple front-end diode rectifier.

Table 1.1 Relative sizes of the input current harmonics in a typical single-phase rectifier supplying a resistive load (input voltage = 115 V,rms, input frequency = 60 Hz, peak-to-peak output voltage ripple = 10% of peak input voltage).

Harmonic number	3	5	7	9	11	13	15	17
$\frac{I_h}{I_1}$ %	95	86	74	60	46	34	26	22

converter between the diode rectifier and the load. In this case, the filtering capacitor is an integral part of the converter and is placed directly across the load. Both buck and boost types of converters can be used for the above purpose.

To make the input power factor equal to unity, the input AC source should see a pure resistance when looking into the input terminals of the diode-rectifier. This resistance emulation is done by controlling the switch in the DC/DC converter used as the intermediate stage between the diode-rectifier and the load. The converter is so controlled that a sinusoidal current in phase with the input voltage is drawn by the rectifier.

Fig. 1.2 shows the basic circuit diagram of a single-phase front-end diode-rectifier circuit with a boost type DC/DC converter as the intermediate stage and a control unit to force the current drawn from the rectifier to follow the rectified voltage waveform. Since the ultimate purpose is to supply a desired DC voltage to the load, a voltage loop will provide the necessary current reference. In fact, the rectified voltage signal which is used as the template for the current is multiplied by a value determined by the output of the voltage controller to fulfill the constant output voltage requirement.

1.3 Literature Survey

Different techniques have been developed for input current waveshaping of front-end diode-rectifiers. These techniques are mostly current-mode control methods, in which the switching frequency is allowed to vary freely in order to fulfill the requirements imposed by the control unit. Techniques are available to let the switching frequency vary by only a small amount from the

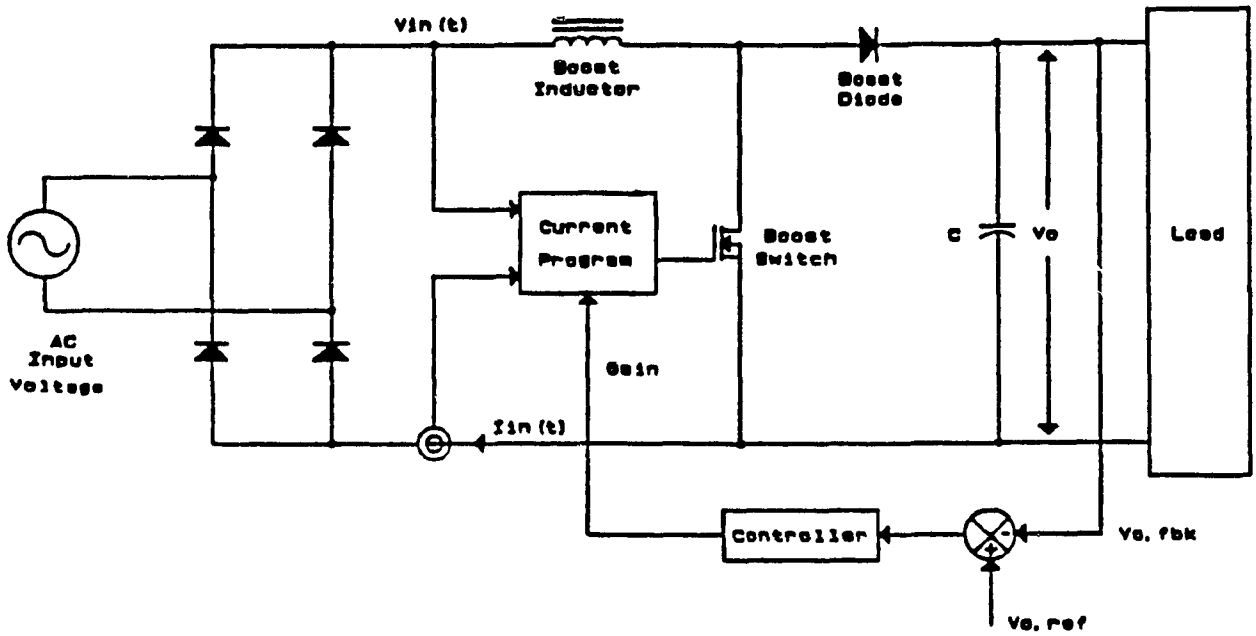

Fig. 1.2 Circuit diagram of a single-phase front-end diode-rectifier with input current waveshaper.

nominal or lock the switching frequency to an external reference. A few computational techniques have also been proposed which work with constant switching frequency and are applicable to the input current waveshaping of front-end diode-rectifiers.

Redl and Sokal have explained the advantages of current-mode control methods over conventional PWM control techniques, and analyzed and compared five different current-mode control techniques in their classic paper [16]. Current-mode control effectively eliminates the 90° phase lag (in the output voltage to control input transfer function of DC/DC converters) due to the filter inductor, by commanding directly the current in the inductor to follow instantaneously the control input. It also eases the application of output current feed forward to obtain very fast correction for load transients, minimizing the deviations of the output voltage. As a result, current-mode control is ideally suited for input current waveshaping purposes.

The most widely used current-mode control method for input current waveshaping is the Bang-Bang Hysteresis (BBH) technique (Fig. 1.3), [3]-[5], [9], [15]-[17]. The hysteresis technique provides the tightest regulation of the inductor current using a simple control circuit. Furthermore, the hysteresis window being a design parameter, free running operation results with the switch frequency being determined by the input and output voltages, the inductor L, and the window size. The varying switching frequency is the serious disadvantage of the hysteresis technique.

"Turn-on" at clock time and "turn-off" at clock time are two different modified versions of the hysteresis technique with constant switching frequency operation [16]. A compensating waveform is needed to obtain stable operation for all duty ratios in the above versions.

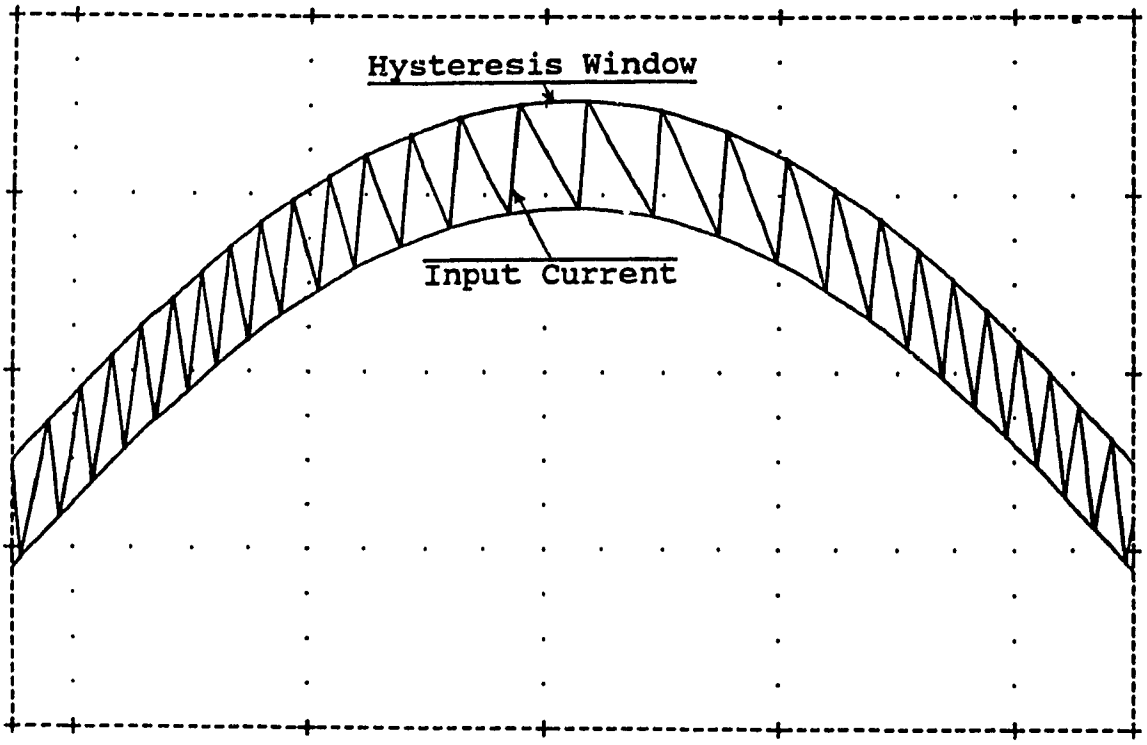

Fig. 1.3 The Bang-Bang Hysteresis input current waveshaping technique: Input current waveform within the hysteresis window.

In the free-running types of current-mode control techniques, the switching frequency can be controlled by varying the "on-time" or the "off-time" of the switch or the width of the hysteresis band. Di Cesare and Gambarara introduce a modified hysteresis technique in which the switching frequency is kept constant by varying the width of the hysteresis band as required, under the control of a phase-locked loop [18]. Another modified hysteresis technique uses two hysteresis comparators with different window sizes to reduce the switching frequency and therefore the losses [17]. The hysteresis window can also be varied in order to improve noise immunity [4].

As seen, any attempt to eliminate or reduce the inherent problems with the hysteresis technique, results in added complexity of the control circuit, compromising the elegance and simplicity of the hysteresis technique.

Current-mode control can be applied in both continuous and discontinuous modes of operation. In a boost type DC/DC converter operating under continuous current conditions, the switching occurs at non-zero voltage and current, and therefore the switching losses can be high. Also, the size of the inductor can be big. In a discontinuous-mode boost converter, the switch turns on at zero current, and therefore the reverse recovery problems associated with free-wheeling diode are eliminated and the switching losses are reduced, but the current ripple is increased.

Zero-voltage switching can be obtained by using an extra switch which in turns adds to the complexity of both power and control circuits [10]. In discontinuous-mode boost converter, the input current contains certain amount of distortion due to the modulation of inductor current discharging time [12].

Along with the current-mode control techniques, there are computational

or predictive methods which predict the way the duty ratio of the switch should vary in order to get the desired waveshape for the input current. They may use the same feedback signals as the conventional methods in addition to some control rule to calculate the required duty ratio to the switch; or they may eliminate the need for the information obtained from some of the feedback signals by predicting them. Computational techniques are known to have longer time responses compared to the conventional methods [19]. They are microprocessor implementable and keep the switching frequency constant. The serious problem with the predictive methods is parameter sensitivity.

A predictive current control strategy with fixed switching frequency has been presented by Wu, Dewan, and Slemon [8] which results in a better switching pattern than hysteresis technique and thus a reduction of harmonics in the line current and lower stress on the switching devices.

1.4 Limitations of the Input Current Waveshaping

The case of input current waveshapers is different from other power processors in that the switching frequency is not the only factor which determines the size and weight of the energy storing elements and the speed of response [2]. The reason lies in the fact that there are basic limitations concerning the amount of stored energy and the speed of response, in input current waveshapers, that are independent of switching frequency.

The first limitation stems from the fact that in the configurations like that shown in Fig. 1.2, a varying electric power is drawn from the input AC source and a fixed amount of power is delivered to the load; therefore it is obvious that the falls and rises in the input power during successive half cycles of the AC input voltage should be taken care of by energy storage

elements in the power processor. It can be shown that the peak stored energy in the power processor should satisfy the following relation in order to fulfill the above requirement [2]:

$$W_{peak} \geq \frac{P_o}{\omega} \tag{1.3}$$

As seen, the minimum amount of stored energy in the processor and thus the minimum size of the energy storage elements is determined by the line frequency and the output power and is independent of the switching frequency.

The problem put forth exists only for single-phase applications. In a three phase application, where the input power is constant, there is no limitation on the minimum size of the energy storing elements.

The second limitation, i.e., low speed of response, can be understood if the two simultaneous tasks of an active input current shaper, i.e., shaping the input current according to the reference obtained from the AC input voltage, and keeping the output voltage at the desired level, are linked together. In fact, to make the output voltage loop fast, its bandwidth should be increased; but if the bandwidth of the above loop is in the order of or higher than twice the line frequency, (which is the frequency of the output voltage ripple), then the voltage loop will respond to the ripple on the output voltage by changing the factor which will be multiplied by the input voltage signal used as the template for the current. In this way, the shape of the input current will be distorted by low order harmonics.

The remedy is to limit the bandwidth of the voltage loop to well below twice the line frequency. This makes the voltage loop extremely slow. As a matter of fact, fast voltage control is sacrificed for fast control or

satisfactory shaping of the input current.

Fast voltage regulation is possible by adding another processor stage (e.g., another boost converter) between the main power processor and the load, but this makes the system more complex and more expensive.

1.5 Scope of the Work Presented

In this thesis, the case of a single-phase front-end diode-rectifier circuit is considered and the power processing stage chosen is a boost type DC/DC converter. A novel active input current waveshaping technique and a computational approach to input current waveshaping are presented and discussed. The switching frequency is constant in both methods. The simulation and experimental results are used to verify the theoretical concepts. The advantages and disadvantages of the methods presented are discussed using the bang-bang hysteresis technique as the base of comparison.

1.6 Summary of the Contents of the Thesis

Chapter 2 discusses design aspects of the bang-bang hysteresis input current waveshaping technique. This provides a base of comparison with a well established method for the techniques presented in the following chapters.

In chapter 3, a novel active input current waveshaping technique, based on the "Error Triangulation Method" will be discussed.

Chapter 4 presents a computational approach to input current waveshaping. The basic scheme and a variation are introduced and discussed.

Chapter 5 makes a comparative evaluation of the techniques discussed in the preceding chapters. Finally chapter 6 contains a summary and conclusions.

CHAPTER 2

BANG-BANG HYSTERESIS CURRENT WAVESHAPING TECHNIQUE

2.1 Introduction

Due to its simple implementation, the bang-bang hysteresis technique is the most widely used current control method for active input current waveshaping. The strength of the method lies in the fact that it provides the tightest instantaneous current regulation using a simple control circuit. Using the bang-bang method, the controlled current remains within a window whose size is a design parameter and fixes the maximum ripple of current.

In the following sections, the principles of operation of bang-bang method and the analysis of the converter using this control technique will be given.

2.2 Principles of Operation

The basic circuit diagram of a single-phase front-end diode-rectifier including a step-up converter controlled by hysteresis technique and used for input current waveshaping purpose is shown in Fig. 2.1.

The goal is to control the boost converter in such a way that the inductor current, i_L , follows as closely as possible the current reference, $i_{L,ref}$. For this purpose, the inductor current signal, $i_{L,fbk}$, is compared with a weighted signal whose shape is determined by the rectified voltage signal, $|v_s|$, and its amplitude is fixed by the output voltage controller

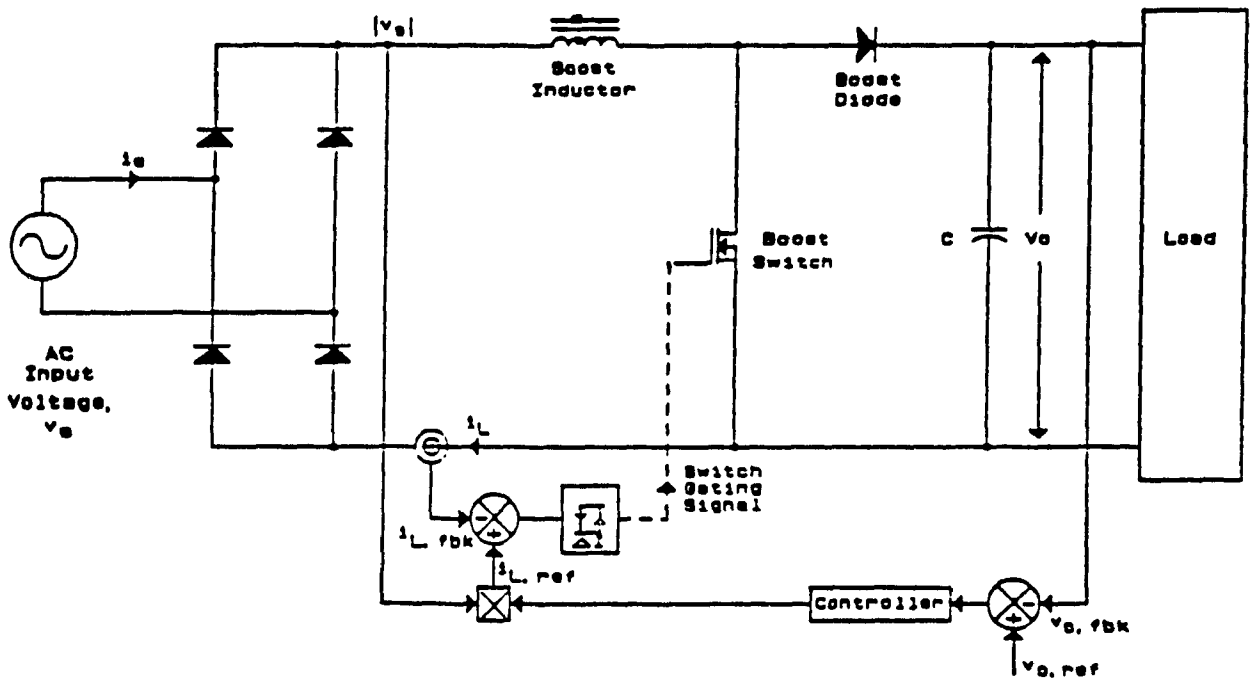

Fig. 2.1 A single-phase front-end diode-rectifier input-current waveshaping circuit controlled by hysteresis technique.

which is responsible for keeping the output voltage at a constant level. If the error is within $\pm \frac{\Delta I}{2}$, (ΔI being the width of the hysteresis window), no switching occurs; but as soon as the error reaches $+ \frac{\Delta I}{2}$ or $- \frac{\Delta I}{2}$, the switch is operated and the topological mode of the power circuit changes. The equivalent circuits for the two different modes of operation of the power circuit, assuming the load to be resistive, are shown in Fig. 2.2 .

If the switch is ON, the, inductor current will increase and there is a moment at which the error between $i_{L,ref}$ and $i_{L,fbk}$ reaches $\frac{\Delta I}{2}$ (Fig.2.3). At this moment, the switch is turned off and the current starts decreasing until the error reaches $- \frac{\Delta I}{2}$. Now it is time for the switch to be turned on again. As a result, the error is always kept within $\pm \frac{\Delta I}{2}$, and centered about zero.

Fig. 2.4 shows the inductor current waveform over a half cycle of the AC input voltage. The window within which the current is maintained is shown as well.

As seen, hitting either of the two current limits (upper or lower), causes a mode change and current slope reversal. As a result, current is always kept within the hysteresis window and centered about the desired waveshape, resulting in a tight current regulation.

As it is observed from Fig. 2.3 and Fig. 2.4, the converter controlled by hysteresis technique has a free running operation; i.e., only the window size is dictated by the control unit and the switching frequency is varying freely as a function of the input and output voltages as well as the inductor value, L, to fulfill the requirement imposed by the control circuit. It can be seen by inspection that as ΔI (i.e., the window size,) is decreased, the frequency of switching will increase and vice versa. The relation between the switching

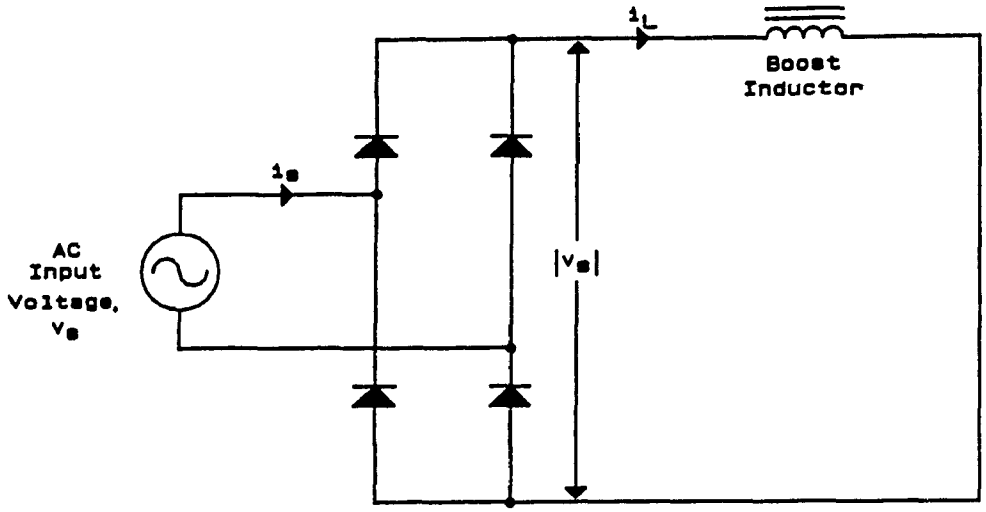

a) Mode 1: Switch ON

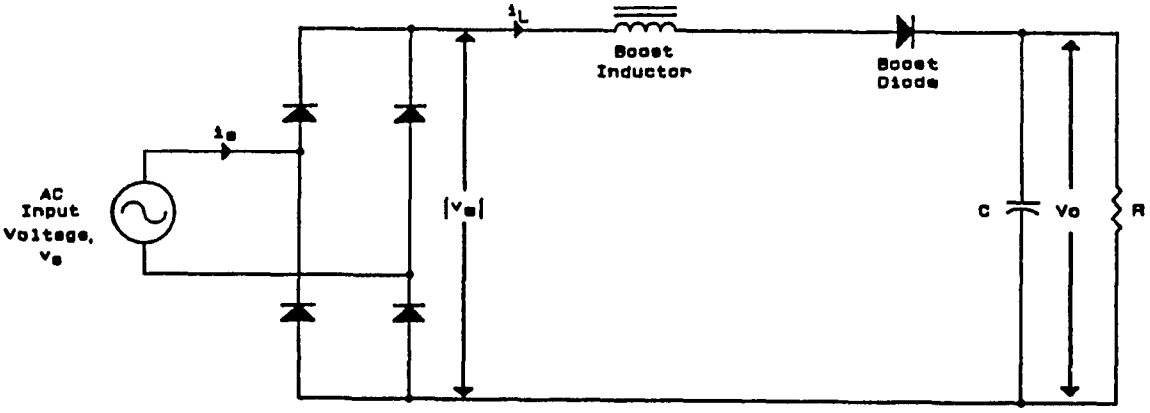

b) Mode 2: Switch OFF

Fig. 2.2 Topological modes of operation of the power circuit of Fig. 2.1 .

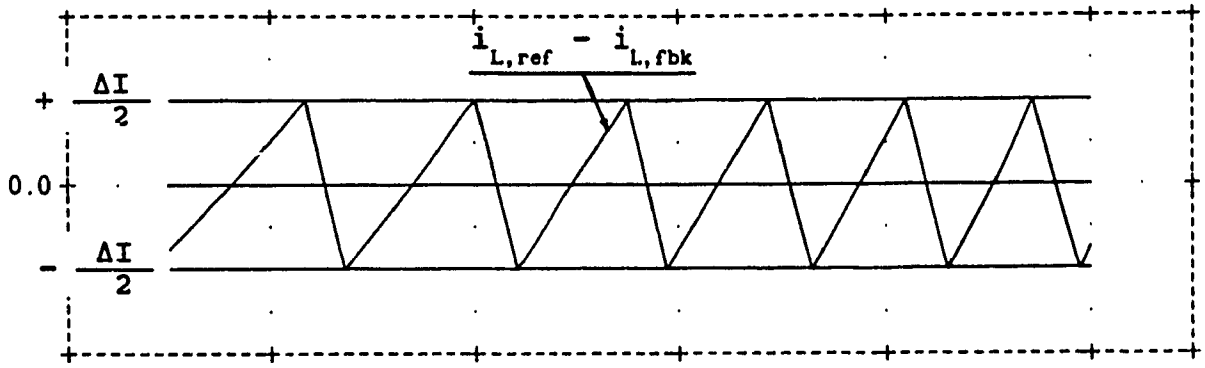

Fig. 2.3 The error, $i_{L,ref} - i_{L,fbk}$, within the window of width ΔI.

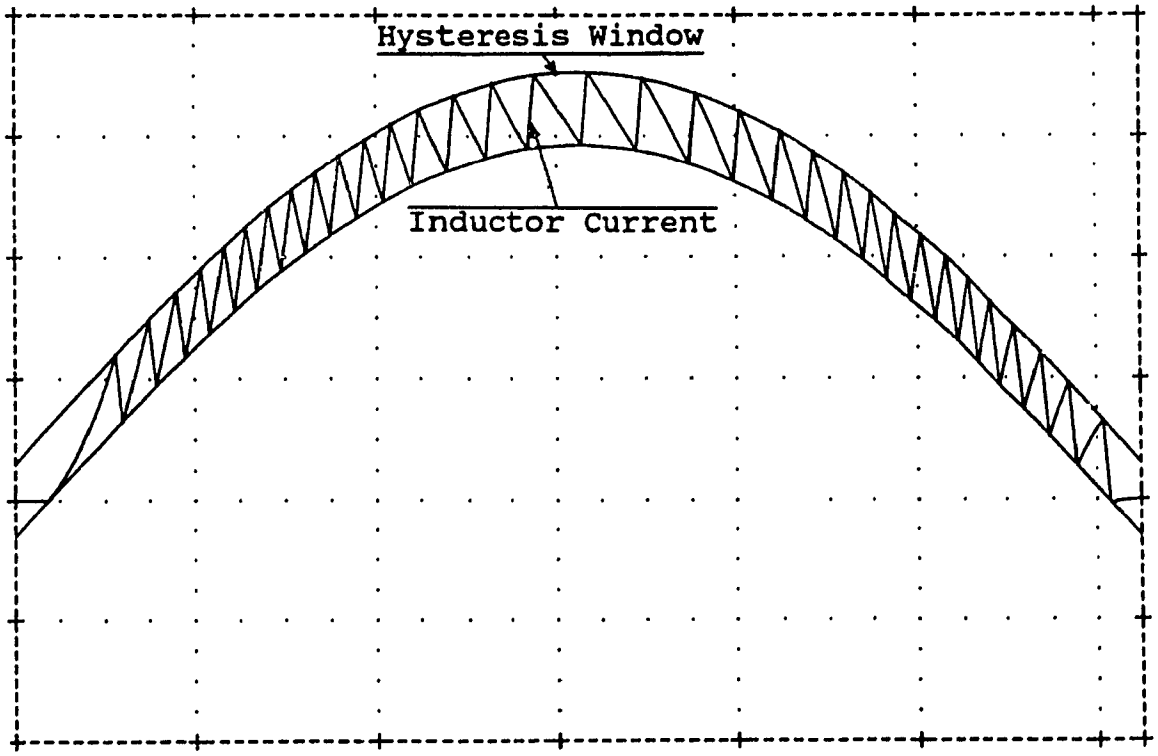

Fig. 2.4 The inductor current inside the hysteresis window.

frequency and input and output voltages, L, and ΔI will be discussed further in the following section.

2.3 Converter Analysis

Fig. 2.5 shows the inductor current and the hysteresis window for a few switching periods during the positive half cycle of the AC input voltage.

The current reference is $I_m \sin \omega t$, the upper limit $I_m \sin \omega t + \frac{\Delta I}{2}$, and the lower limit $I_m \sin \omega t - \frac{\Delta I}{2}$ (ΔI being the hysteresis window size).

During the time interval $t_1 \leq t \leq t_2$, the boost switch is ON and the power circuit is in mode 1 (Fig. 2.2.a). The slope of the current during this period is:

$$m_{ON} = \frac{V_m \sin \omega t}{L} \qquad (2.1)$$

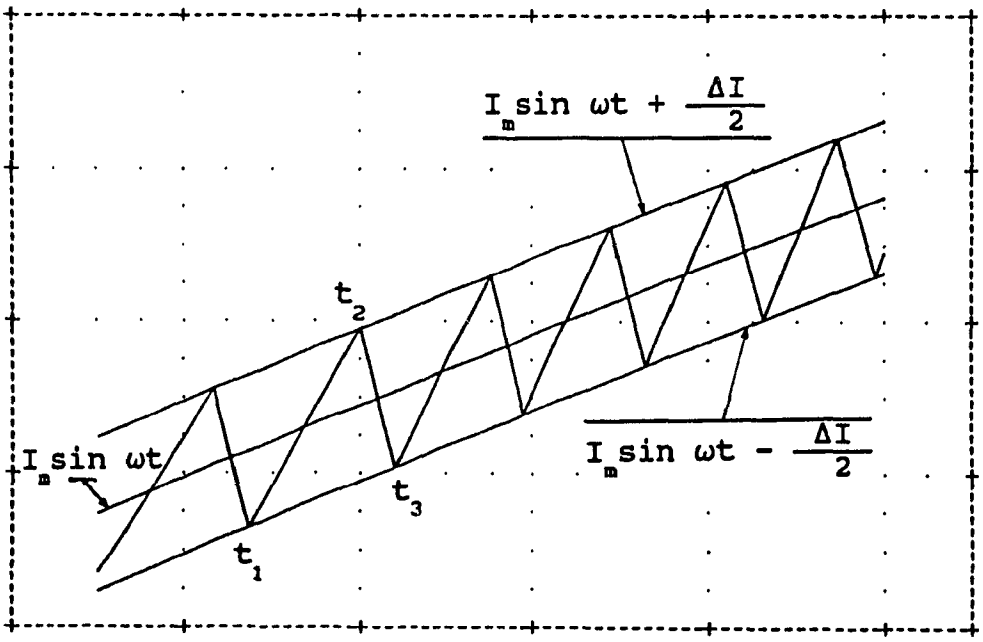

Fig. 2.5 The inductor current within hysteresis window.

and the average slope during the interval [t_1,t] will be:

$$m_{ON,ave} = \frac{1}{t-t_1} \int_{t_1}^{t} \frac{V_m \sin \omega t}{L} dt$$

$$= \frac{V_m}{(t-t_1)\,\omega L} (\cos \omega t_1 - \cos \omega t) \qquad (2.2)$$

Therefore, the inductor current can be expressed as follows: [20]

$$i_L(t) \cong i_L(t_1) + \frac{V_m}{(t-t_1)\,\omega L} (\cos \omega t_1 - \cos \omega t)(t - t_1)$$

$$= i_L(t_1) + \frac{V_m}{\omega L} (\cos \omega t_1 - \cos \omega t) \qquad (2.3)$$

During the time interval in which the circuit is operating in mode 1, electrical energy is stored in the inductor and the output capacitor is responsible for supplying power to the resistive load. Assuming that the ON - period of the switch is short compared with the period of the AC input voltage and the time constant of the output filter is large, the change in the output voltage will be negligible in this period of time and the output voltage can be taken constant during the ON - period of the switch.

The ON - period of the switch, t_{ON} , can be derived from Eqn. (2.3) putting $t = t_2$ and substituting $i_L(t_2)$ and $i_L(t_1)$ by their equivalents, i.e., $I_m \sin \omega t + \frac{\Delta I}{2}$ and $I_m \sin \omega t - \frac{\Delta I}{2}$, respectively.

$$I_m \sin \omega t_2 + \frac{\Delta I}{2} = I_m \sin \omega t_1 - \frac{\Delta I}{2} + \frac{V_m}{\omega L} (\cos \omega t_1 - \cos \omega t_2) \qquad (2.4)$$

Eqn. (2.4) can be changed to

$$\Delta I = I_m (\sin \omega t_1 - \sin \omega t_2) + \frac{V_m}{\omega L} (\cos \omega t_1 - \cos \omega t_2)$$

$$= 2I_m \cos \frac{\omega (t_1+t_2)}{2} \sin \frac{\omega (t_1-t_2)}{2} +$$

$$\frac{2V_m}{\omega L} \sin \frac{\omega (t_1+t_2)}{2} \sin \frac{\omega (t_2-t_1)}{2} \qquad (2.5)$$

Replacing $\frac{t_1+t_2}{2}$ by t, and t_2-t_1 by t_{ON} (the ON - period of the switch), and solving for t_{ON} , the following approximate relation results:

$$t_{ON} \cong \frac{2}{\omega} \sin^{-1} \frac{\Delta I}{2(\frac{V_m}{\omega L} \sin \omega t - I_m \cos \omega t)} \qquad (2.6)$$

Remembering that for very small angles, the sine is approximately equal to the value of the angle in radians, and knowing that based on the assumption made before concerning the value of t_{ON}, $\sin^{-1}$ in Eqn. (2.6) is very small, the following simpler relation can be obtained for t_{ON}:

$$t_{ON} \cong \frac{L \Delta I}{V_m \sin \omega t - \omega L I_m \cos \omega t} \qquad (2.7)$$

During the time interval $t_2 \leq t \leq t_3$, the boost switch is OFF and the power circuit is in mode 2 (Fig. 2.2.b). The slope of the inductor current during this period is

$$m_{OFF} = \frac{v_s - V_o}{L} = \frac{V_m \sin \omega t - V_o}{L} \qquad (2.8)$$

and the average slope during the interval $[t_2, t]$ will be

$$m_{OFF,ave} = \frac{1}{t-t_2} \int_{t_2}^{t} \frac{V_m \sin \omega t - V_o}{L} dt$$

$$= \frac{1}{t-t_2} \left[\frac{V_m}{\omega L} (\cos \omega t_2 - \cos \omega t) - \int_{t_2}^{t} \frac{V_o}{L} dt \right] \qquad (2.9)$$

Assuming V_o to be constant,

$$m_{OFF} \cong \frac{V_m}{\omega L(t-t_2)} (\cos \omega t_2 - \cos \omega t) - \frac{V_o}{L} \qquad (2.10)$$

The inductor current can then be expressed as follows: [20]

$$i_L(t) \cong i_L(t_2) + \left[\frac{V_m}{\omega L(t-t_2)} (\cos \omega t_2 - \cos \omega t) - \frac{V_o}{L} \right](t-t_2)$$

$$= i_L(t_2) + \frac{V_m}{\omega L} (\cos \omega t_2 - \cos \omega t) - \frac{V_o}{L} (t-t_2) \qquad (2.11)$$

During the time interval in which the circuit is operating in mode 2, the stored energy in the inductor is released. Both this energy and the energy coming from AC supply are then directed towards the output circuitry. The output capacitor will gain the voltage lost during t_{ON} and gets ready to supply power to the load during the next ON - period of the switch. Again, because the OFF - period of the switch is comparatively short and the output capacitor value is high, the voltage change during t_{OFF} is negligible and the output voltage can be taken to be constant.

The OFF - period of the switch, t_{OFF} , can be derived from Eqn. (2.11) taking $t=t_3$ and substituting $i_L(t_3)$ and $i_L(t_2)$ by their equivalents, i.e.,

$I_m \sin \omega t_3 - \frac{\Delta I}{2}$ and $I_m \sin \omega t_2 + \frac{\Delta I}{2}$, respectively.

$$I_m \sin \omega t_3 - \frac{\Delta I}{2} = I_m \sin \omega t_2 + \frac{\Delta I}{2} + \frac{V_m}{\omega L} (\cos \omega t_2 - \cos \omega t_3) - \frac{V_o}{L} (t_3 - t_2) \tag{2.12}$$

Eqn. (2.12) can be changed to

$$\begin{aligned} -\Delta I &= I_m (\sin \omega t_2 - \sin \omega t_3) + \frac{V_m}{\omega L} (\cos \omega t_2 - \cos \omega t_3) - \frac{V_o}{L} (t_3 - t_2) \\ &= 2 \sin \frac{\omega (t_3 - t_2)}{2} \left[\frac{V_m}{\omega L} \sin \frac{\omega (t_2 + t_3)}{2} - I_m \cos \frac{\omega (t_2 + t_3)}{2} \right] \\ &\quad - \frac{V_o}{L} (t_3 - t_2) \end{aligned} \tag{2.13}$$

Replacing $\frac{t_2 + t_3}{2}$ by t and $t_3 - t_2$ by t_{OFF}, the following approximate relation results:

$$\Delta I = \frac{V_o}{L} t_{OFF} - 2 \sin \frac{\omega t_{OFF}}{2} \left(\frac{V_m}{\omega L} \sin \omega t - I_m \cos \omega t \right) \tag{2.14}$$

Obviously, t_{OFF} can be found from Eqn. (2.14), using an iterative method, when all other parameters are known.

Again a simpler expression for t_{OFF} can be found using the approximation:

$$\sin \frac{\omega t_{OFF}}{2} = \frac{\omega t_{OFF}}{2}$$

Therefore,

$$t_{OFF} = \frac{L \Delta I}{V_o - (V_m \sin \omega t - \omega L I_m \cos \omega t)} \tag{2.15}$$

As Eqns. (2.6) and (2.7) show, t_{ON} depends on ω, ΔI, L, the input voltage

and the current reference values, while t_{OFF} depends on the same values plus the output voltage level, as indicated by Eqns. (2.14) and (2.15). Having been given the parameters affecting t_{ON} and t_{OFF}, these two quantities and as a result, the switching period, $t_{ON} + t_{OFF}$, and the switching frequency, $1/(t_{ON} + t_{OFF})$, can be found as functions of time.

Eqns. (2.7) and (2.15) yield

$$T_{sw} = t_{ON} + t_{OFF} = \frac{L\ \Delta I\ V_o}{(V_m \sin \omega t - \omega L I_m \cos \omega t)\left[V_o - (V_m \sin \omega t - \omega L I_m \cos \omega t)\right]} \tag{2.16}$$

Therefore,

$$f_{sw} = \frac{(V_m \sin \omega t - \omega L I_{fn} \cos \omega t)\left[V_o - (V_m \sin \omega t - \omega L I_m \cos \omega t)\right]}{L\ \Delta I\ V_o} \tag{2.17}$$

Fig. 2.6 shows the variations of the switching frequency vs. time during a full cycle of the AC input voltage for: V_m = 1.414 p.u., V_o = 1.597 p.u., ΔI = 0.438 p.u., I_m = 4.384 p.u., f_{IN} = 1 p.u., and L = 0.026 p.u. .

Fig. 2.6 indicates that the switching frequency varies in a wide range below and above its average value during each half cycle of the AC input voltage. The average switching frequency varies according to the changes in the input and output voltages as well as the hysteresis window size. Even though the average value of the switching frequency gives some idea about the operation of the switch, it should be kept in mind that the instantaneous value of the switching frequency can reach very high levels while the average value is appropriate for the switch.

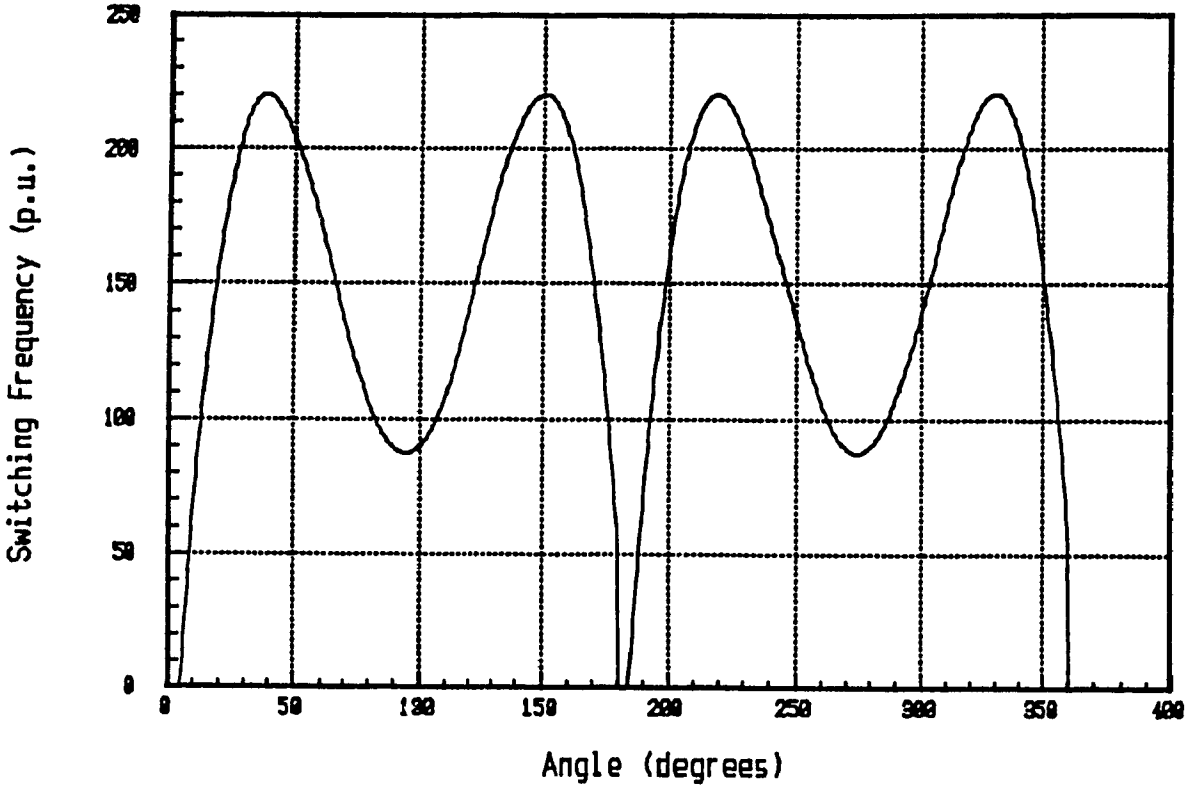

Fig. 2.6 Switching frequency variations during one cycle of the AC input voltage (V_m = 1.414 p.u., V_o = 1.597 p.u., ΔI = 0.438 p.u., I_m = 4.384 p.u., f_{in} = 1 p.u., and L = 0.026 p.u.).

To investigate the effects of changes in ΔI and the output voltage on switching frequency, the average values for the switching frequency over a half cycle of the AC input voltage will be derived, using Eqn. (2.17):

$$f_{sw,ave} \cong \frac{1}{T/2}\int_0^{T/2} \frac{(V_m \sin \omega t - \omega L I_m \cos \omega t)\left[V_o - (V_m \sin \omega t - \omega L I_m \cos \omega t)\right]}{L\,\Delta I\,V_o}$$

$$= \frac{4V_o V_m - \pi(\omega^2 L^2 I_m^2 + V_m^2)}{2\pi L\,\Delta I\,V_o} \qquad (2.18)$$

As it can be observed from the above approximate expression, the average switching frequency is almost insensitive to the variations of the amplitude of the current reference ($f_{sw,ave}$ = 526.3 p.u. for 0.1 p.u. current reference and $f_{sw,ave}$ = 525.1 p.u. for 1.0 p.u. current reference, with V_m = 1.414 p.u., V_o = 1.913 p.u., ΔI = 0.113 p.u., f_{IN} = 1 p.u., and L = 0.04 p.u.), but is affected by changes in V_m, V_o, L, and ΔI. Assuming V_m and L to be constant values, the effects of V_o and ΔI on average switching frequency can be investigated.

Fig. 2.7 shows the variations of the average switching frequency vs. V_o for: V_m = 1.414 p.u., ΔI = 0.438 p.u., I_m = 4.384 p.u., and L = 0.026 p.u. . It indicates that the switching frequency is considerably affected by the output voltage changes. The variations in the DC component of the output voltage can be attributed to load changes. When a load change takes place at a speed higher than the speed of the output voltage control loop (which is generally slow in the type of configuration considered), the amplitude of the inductor current cannot be adjusted during the same half cycle of the AC input voltage

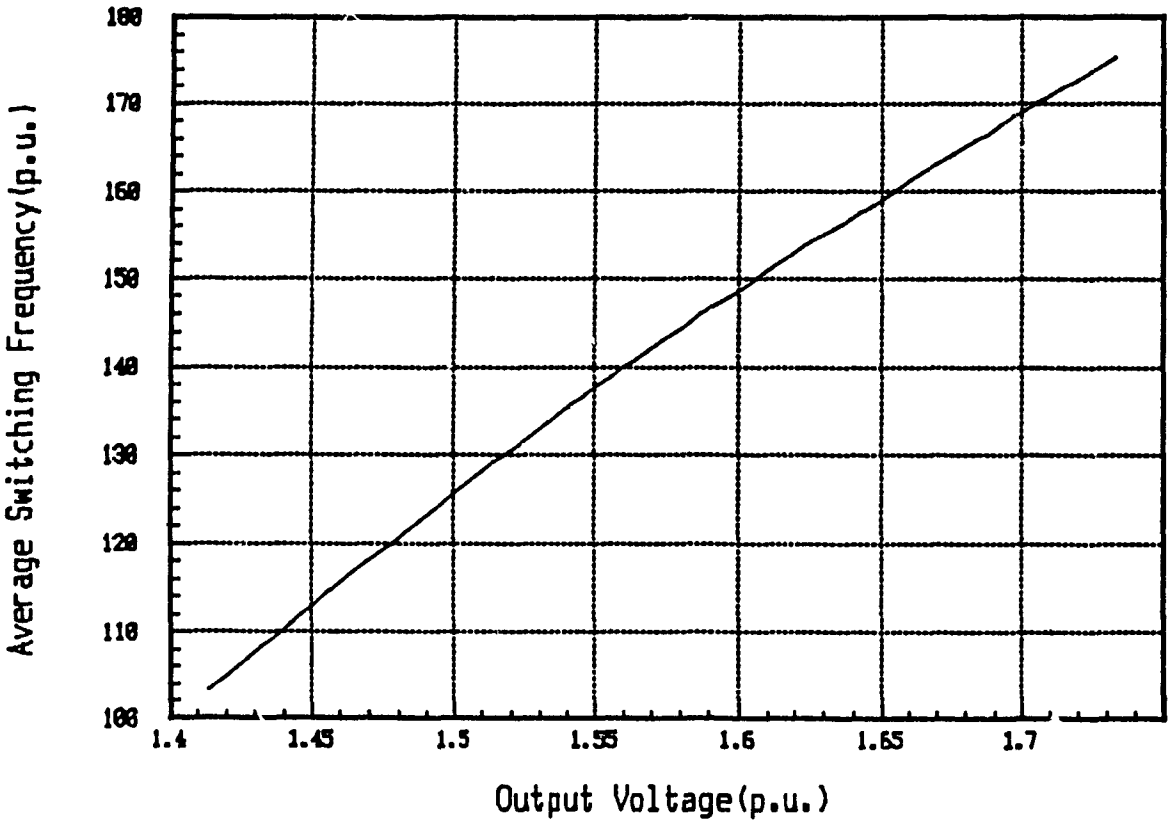

Fig. 2.7 Average switching frequency vs. output voltage (V_m = 1.414p.u., ΔI = 0.438 p.u., I_m = 4.384 p.u., and L = 0.026 p.u.).

as that in which the load change occurred, to restore the desired output voltage level. Therefore, the voltage rise (for load decrease) or the voltage dip (for load increase) will stay long enough for the switch to experience a new average switching frequency. The instantaneous switching frequency can have a large deviation around the average value in a half cycle of the AC input voltage, i.e., the switching frequency can reach very high values while the average value is not very high, and this can cause high switching losses if not permanent damage to the switch.

Fig. 2.8 shows the variations of the average switching frequency vs. ΔI for: V_m = 1.414 p.u., V_o = 1.597 p.u., I_m = 4.384 p.u., and L = 0.026 p.u. .

Fig. 2.8 indicates that higher average switching frequency (and therefore higher switching losses), is the price for lower inductor current ripple.

It was said before that in hysteresis method, the controlled current hits the upper and the lower limits successively in such a way that the current is always kept within a band. In fact, for this to be true, the slope of the current and the size of the current reference and the hysteresis window cannot assume any arbitrary value. For example, it is possible that because of the proximity of the current slope to the slope of the reference, current intersects one of the limits more than one time without hitting the other limit in between. It is obvious that hitting one limit does not result in a switching unless it has been preceded by hitting the other limit. Therefore, in such a case control is lost temporarily and current will not remain within the window for a while. So, in order to obtain a tight current control, the values of current slope, and the size of the reference and the window should be matched with each other.

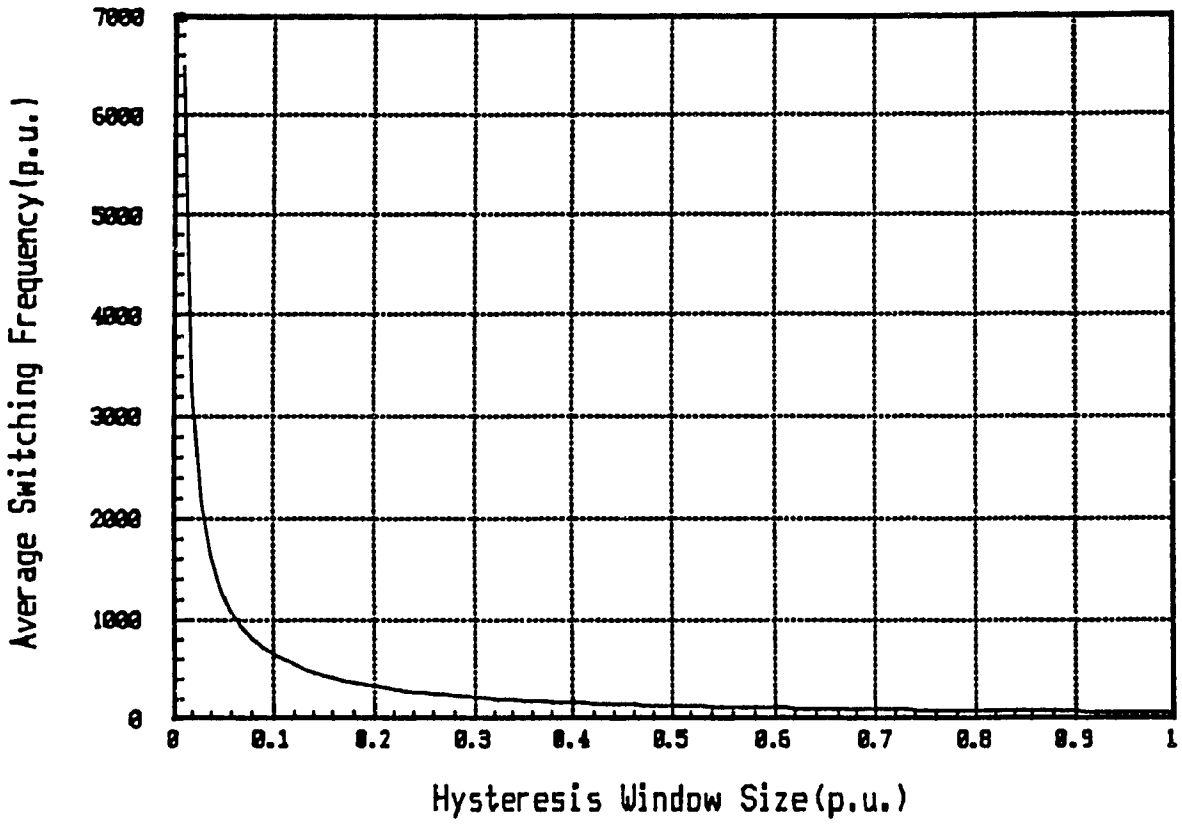

Fig. 2.8 Average switching frequency vs. hysteresis window size (V_m = 1.414 p.u., V_o = 1.597 p.u., I_m = 4.384 p.u., and L = 0.026 p.u.).

2.4 Ratings of the Converter Components

In this section, the voltage and current ratings of the components used in the power circuit of Fig. 2.1, i.e., the rectifier diodes, the boost inductor, the boost switch, the boost diode, and the output capacitor will be found in per unit of the rated values. Throughout this section,

$$1 \text{ p.u. } W = P_{rated} ;$$

$$1 \text{ p.u. } V = v_{s,rms,rated} ;$$

$$V_o = a\, v_{s,peak} ;$$

and

$$v_{or,p-p} = rV_o , \tag{2.19}$$

where V_o and v_{or} are the DC and the ripple components of the output voltage, respectively.

It follows from (2.19) that

$$1 \text{ p.u. } A = \frac{P_{rated}}{v_{s,rms,rated}} = i_{s,rms,rated} \tag{2.20}$$

2.4.1. Rectifier Diode Ratings

Each of the front-end rectifier diodes experiences the input current, i_s, for only a half cycle of the AC input voltage; therefore,

$$i_{rD,peak} = i_{s,peak} = 1.414 \text{ p.u.};$$

$$i_{rD.ave} = \frac{1}{\Pi} i_{s,peak} = \frac{1.414}{\Pi} \text{ p.u.} = 0.45 \text{ p.u.};$$

and

$$i_{rD,rms} = \left[\frac{1}{T} \int_0^{T/2} (i_{s,peak} \sin \omega t)^2 \, dt \right]^{1/2}$$

$$= \frac{1}{2} i_{s,peak} = 0.707 \text{ p.u.} \quad . \tag{2.21}$$

The maximum reverse voltage experienced by each rectifier diode will be

$$v_{rev,peak} = v_{s,peak} = 1.414 \text{ p.u.} \quad . \tag{2.22}$$

2.4.2. Boost Inductor Ratings

It is clear that

$$i_L = |i_s| \tag{2.23}$$

therefore,

$$i_{L,rms} = |i_s|_{,rms} = i_{s,rms} = 1 \text{ p.u.}; \tag{2.24}$$

Also,

$$i_{L,peak} = i_{s,peak} = 1.414 \; i_{s,rms} = 1.414 \text{ p.u.}; \tag{2.25}$$

and

$$i_{L,ave} = i_{L,DC} = |i_s|_{,ave} = 2/\Pi \; i_{s,peak} = 0.9 \text{ p.u.} \quad . \tag{2.26}$$

The maximum voltage is placed across the inductor when $v_s = 0$; therefore,

$$v_{L,max} = V_o = a\, v_{s,peak} = 1.414\ a\ v_{s,rms} = 1.414\ a\ \text{p.u.}\ . \qquad (2.27)$$

2.4.3. Boost Diode Ratings

It is obvious that

$$i_{D,peak} = i_{L,peak} = i_{s,peak} = 1.414\ \text{p.u.}\ . \qquad (2.28)$$

To obtain $i_{D,ave}$ and $i_{D,rms}$, an expression in time is needed for i_D. Fourier analysis of the diode current shows that (considering only the DC and the fundamental components of i_D)

$$i_D \cong K\ (1 - \cos 2\omega t) \qquad (2.29)$$

Since it is known that $i_{D,peak} = i_{s,peak}$, K can be found to be

$$K = i_{s,peak}/2 \qquad (2.30)$$

and therefore,

$$i_D \cong \frac{i_{s,peak}}{2}\ (1 - \cos 2\omega t) \qquad (2.31)$$

Having found a time expression for i_D, and assuming T to be the period of the AC input voltage, $i_{D.rms}$ can be found as follows:

$$i_{D,rms} = \left[\frac{2}{T} \int_0^{T/2} \left[\frac{i_{s,peak}}{2}\ (1 - \cos 2\omega t) \right]^2 dt \right]^{1/2}$$

$$= 0.612\ i_{s,peak} = 0.866\ \text{p.u.}\ . \qquad (2.32)$$

Finally, the diode average current is found to be

$$i_{D,ave} = i_{D,DC} = \frac{i_{s,peak}}{2} = 0.707\ \text{p.u.}\ . \qquad (2.33)$$

2.4.4. Boost Switch Ratings

It is clear that the maximum voltage is placed across the switch during its OFF-period and is equal to the output voltage:

$$v_{sw,peak} = V_o = 1.414 \text{ a p.u. .} \tag{2.34}$$

To find the current ratings of the boost switch, a time expression for the current through the switch is needed. In fact,

$$i_{sw} = i_L - i_D \tag{2.35}$$

During the positive half cycle of the AC input voltage, the above relation becomes

$$i_{sw} \cong i_{s,peak} \sin \omega t - \frac{i_{s,peak}}{2} (1 - \cos 2\omega t) \tag{2.36}$$

Now, $i_{sw,peak}$, $i_{sw,ave}$, and $i_{sw,rms}$ can be found as follows:

$i_{sw,peak}$ is found by equating the derivative of i_{sw} to zero.

$$\frac{di_{sw}}{dt} = \omega i_{s,peak} \cos \omega t (1 - 2\sin \omega t) = 0 \tag{2.37}$$

The maximum for i_{sw} occurs at $\omega t = 30$ degs. and is

$$i_{sw,peak} = \frac{i_{s,peak}}{4} = 0.354 \text{ p.u. .} \tag{2.38}$$

$i_{sw,ave}$ is found to be

$$i_{sw,ave} = \frac{2}{\Pi} i_{s,peak} - \frac{1}{2} i_{s,peak} = \frac{4 - \Pi}{2\Pi} i_{s,peak}$$

$$= 0.193 \text{ p.u. .} \tag{2.39}$$

Finally, $i_{sw,rms}$ is found in the following way:

$$i_{sw.rms} = \left[\frac{2}{T} \int_0^{T/2} \left[i_{s,peak} \sin \omega t - \frac{i_{s,peak}}{2} (1 - \cos 2\omega t) \right]^2 dt \right]^{1/2}$$

$$= \left[\frac{21\pi - 64}{24} \right]^{1/2} i_{s,peak} = 0.229 \text{ p.u.} \quad . \qquad (2.40)$$

2.4.5. Output Capacitor Ratings

Fourier analysis of the output capacitor voltage shows that (considering only the DC and the fundamental components of V_o)

$$v_o \cong V_o - v_{or,peak} \sin 2\omega t \qquad (2.41)$$

Assuming that the peak - to - peak ripple voltage is related to the DC component of the output voltage, through the relation

$$v_{or,p-p} = 2v_{or,peak} = rV_o \qquad (2.42)$$

the output voltage can be expressed as

$$v_o = V_o - \frac{rV_o}{2} \sin 2\omega t \qquad (2.43)$$

Therefore,

$$v_{o,ave} = v_{o,DC} = V_o = 1.414 \text{ a p.u.};$$

$$v_{o,peak} = V_o + \frac{rV_o}{2} = \left(1 + \frac{r}{2}\right) 1.414 \text{ a p.u.}; \qquad (2.44)$$

and

$$v_{o,rms} = \left[\frac{2}{T} \int_0^{T/2} \left(V_o - \frac{rV_o}{2} \sin 2\omega t \right)^2 dt \right]^{1/2}$$

$$= \left[1 + \frac{r^2}{8} \right]^{1/2} V_o = \left[1 + \frac{r^2}{8} \right]^{1/2} 1.414 \text{ a p.u. .} \qquad (2.45)$$

Having a time expression for the output capacitor voltage, the capacitor current can be found:

$$i_C = C \frac{dv_C}{dt} = C \frac{dv_o}{dt} = - rV_o \omega \cos 2\omega t \qquad (2.46)$$

Therefore,

$$i_{C,rms} = \left[\frac{2}{T} \int_0^{T/2} \left(- rV_o \omega \cos 2\omega t \right)^2 dt \right]^{1/2}$$

$$= \frac{rV_o \omega}{\sqrt{2}} = r\omega a \text{ p.u. .} \qquad (2.47)$$

2.5. Design Example

The power circuit is designed according to the following specifications:

Output Power (P_o) = 1000 W;

Output Voltage (V_o) = 220 V;

Output Voltage Ripple ≤ 2% ;

Input Voltage (v_s) = 115 V,rms ;

Input Current THD ≤ 5% ;

Unity Input Power Factor;

Line Frequency = 60 Hz ;

and

$$\text{Maximum Switching Frequency} = 40 \text{ kHz} .$$

The base values are defined as:

$$P_B = P_o = 1000 \text{ VA};$$

$$V_B = v_s = 115 \text{ V,rms} ;$$

$$I_B = P_B / V_B = 1000/115 = 8.7 \text{ A,rms} ;$$

$$Z_B = V_B / I_B = 115/8.7 = 13.22 \ \Omega ;$$

$$f_B = 60 \text{ Hz} ;$$

$$L_B = \frac{13.22}{(2\Pi)\ (60)}\ 10^6 = 35062.87 \ \mu\text{H} ;$$

and

$$C_B = \frac{1}{(13.22)\ (2\Pi)\ (60)}\ 10^6 = 200.67 \ \mu\text{F} .$$

Given the above specifications and base values, and assuming the converter to be lossless,

$$i_s = 1 \text{ p.u.} ;$$

$$V_o = 1.91 \text{ p.u.} ;$$

and the load resistance,

$$R_L = 3.65 \text{ p.u.} .$$

The corresponding design specifications will then dictate the size of the boost inductor and the output capacitor.

2.5.1 Design of L

Eqn. (2.17) gives an approximate expression for the switching frequency. At the maximum, the time derivative of the switching frequency

function is zero. Equating the derivative with respect to time of f_{sw} to zero, the following equation results:

$$V_o V_m \cos \omega t + \omega L V_o I_m \sin \omega t + (\omega^2 L^2 I_m^2 - V_m^2) \sin 2\omega t + 2\omega L V_m I_m \cos 2\omega t = 0 \tag{2.48}$$

To guarantee that the inductor current will remain within the hysteresis window, a constraint should be put on the value of the inductance according to the size of the window. Fig. 2.9 shows that for the current to stay inside the window, its slope at the moment when it touches the lower limit for the first time, should be at least equal to the slope of the sinusoidal reference at the same moment. Since the equation of the lower limit is $I_m \sin \omega t - \Delta I/2$, the moment the current touches this limit for the first time will be given by

$$\omega t_1 = \sin^{-1} \frac{\Delta I}{2 I_m} \tag{2.49}$$

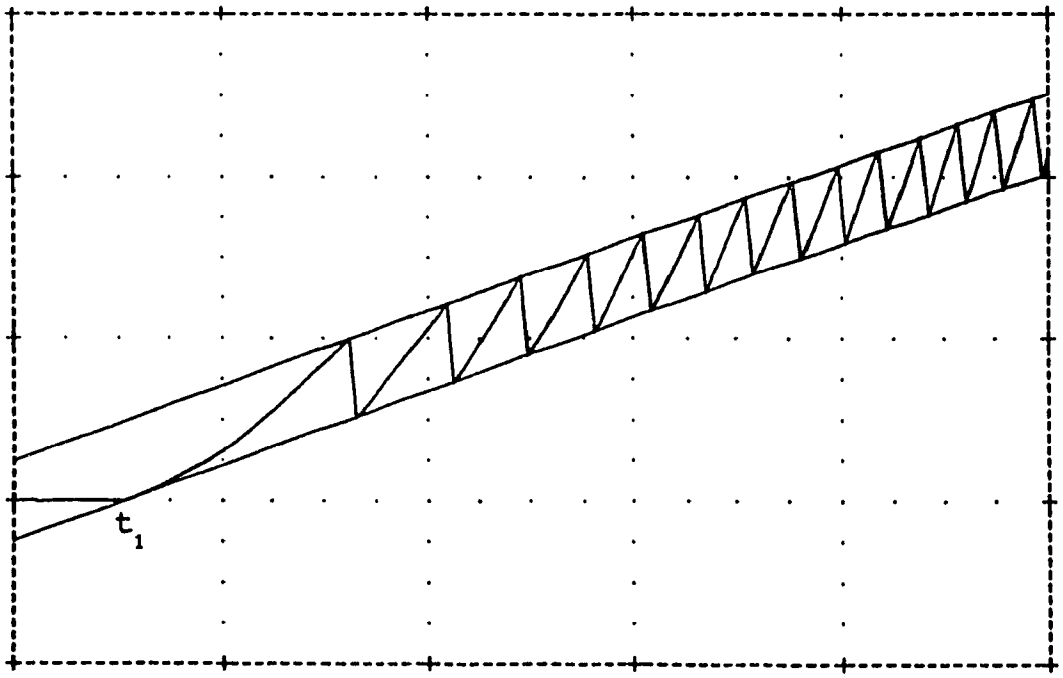

Fig. 2.9 The inductor current within the hysteresis window.

The slope of the current at this moment is

$$m(\omega t_1) = \frac{v_s(\omega t_1)}{L} = \frac{V_m \Delta I}{2 I_m L} \tag{2.50}$$

The slope of the sinusoidal reference at the same time will be

$$m_{sine}(\omega t_1) = \omega I_m \cos \omega t_1 = \frac{\omega}{2} \left[4I_m^2 - (\Delta I)^2 \right]^{1/2} \tag{2.51}$$

Equating (2.50) and (2.51), the following relation results:

$$L = \frac{V_m \Delta I}{\omega I_m \left[4I_m^2 - (\Delta I)^2 \right]^{1/2}} \tag{2.52}$$

The above equation gives the maximum value of L for which the inductor current won't go out of the window of size ΔI. To find the proper value for L Eqns. 2.17, 2.48, and 2.52 should be solved simultaneously using the design specifications. After several iterations, L is found to be

$$L = 1.399 \text{ mH} = 0.04 \text{ p.u.}$$

ΔI can be found from Eqn. 2.52 to be

$$\Delta I = 0.983 \text{ A} = 0.113 \text{ p.u.}$$

Choosing a lower value for L, results in a higher maximum switching frequency for the same ΔI.

Using the values found for L and ΔI, the specification for the input current THD may not be met. In this case, a second order input filter will be necessary to decrease the THD to the allowable level.

2.5.2 Design of C

To find the value of C for a desired output voltage ripple, It is noted that the capacitor - resistor combination at the output of the converter, acts as a low pass filter for the current through the boost diode. This current can be thought of as being supplied by a current source, i_D , whose value is controlled by the output voltage controller and is of sinusoidal nature (considering only its DC and fundamental components):

$$i_D \cong \frac{i_{s,peak}}{2} (1 - \cos 2\omega t) \tag{2.53}$$

The gain of the filter for the DC component of the current is R_L, while its gain for the AC component is

$$|G_{AC}| = \frac{R_L}{\left[(2R_L C\omega)^2 + 1\right]^{1/2}} \tag{2.54}$$

Therefore,

$$\frac{|G_{AC}|}{G_{DC}} = \frac{1}{\left[(2R_L C\omega)^2 + 1\right]^{1/2}} \tag{2.55}$$

Since the DC component and the amplitude of the fundamental harmonic of i_D are almost the same, the ratio of the peak - to - peak value of the output voltage ripple to the DC component of the output voltage, which is by definition the ripple, will be

$$r = 2 \frac{|G_{AC}|}{G_{DC}} \tag{2.56}$$

and as a result, C will be given by the following relation:

$$C = \frac{(4 - r^2)^{1/2}}{2rR_L\omega} \tag{2.57}$$

To get a ripple of less than 2% , a capacitor with C = 2740 μF (13.65 p.u.) would be adequate.

2.6 Simulation Results

Because of the limited size of the data file generated by the simulation program that can be handled by the postprocessor, a ratio of switching frequency to line frequency lower than the one given in the design example was used for simulation purposes. This also indicates the operation of the bang-bang hysteresis technique clearer.

The design specifications are taken to be

Output Power (P_o) = 1000 W;

Output Voltage (V_o) = 350 V;

Output Voltage Ripple ≤ 2% ;

Input Voltage (v_s) = 219.2 V,rms;

Input Current THD ≤ 5% ;

Unity Input Power Factor;

Line Frequency = 400;

and

Maximum Switching Frequency = 40 kHz.

The base values are chosen to be

$$P_B = P_o = 1000 \text{ VA};$$

$$V_B = v_s = 219.2 \text{ V,rms};$$

$$I_B = P_B / V_B = 1000 / 219.2 = 4.56 \text{ A,rms;}$$

$$Z_B = V_B / I_B = 48.05 \ \Omega;$$

$$f_B = 400 \text{ Hz;}$$

$$L_B = 19.12 \text{ mH}$$

and

$$C_B = 8.28 \ \mu\text{F.}$$

As a result,

$$i_s = 1 \text{ p.u.;}$$

$$V_o = 1.6 \text{ p.u.;}$$

and the load resistance,

$$R_L = 122.5 \ \Omega = 2.55 \text{ p.u. .}$$

Again by solving Eqns.(2.17), (2.48), and (2.52), L is found to be

$$L = 1.8 \text{ mH} = 0.094 \text{ p.u. .}$$

ΔI is then found by Eqn. (2.52) to be

$$\Delta I = 1.21 \text{ A} = 0.265 \text{ p.u. .}$$

Furthermore, by Eqn. (2.57), C is found to be

$$C = 162.4 \ \mu\text{F} = 19.6 \text{ p.u. .}$$

Fig. 2.10 shows the simulation results for one cycle of the AC input voltage. The frequency spectrum of the input current is shown in Fig. 2.11.

As shown in Fig. 2.11, the current harmonics are spread all over the frequency spectrum. This makes the task of input current filtering extremely hard. For the case considered, the THD of the input current is found to be 8.5%, using the basic formula for THD and the amplitudes of the current harmonics. But the input current THD is restricted by the design specifications to be less than or equal to 5% . This means an input filter is necessary to take care of the harmonic distortion in excess of 5% . In such

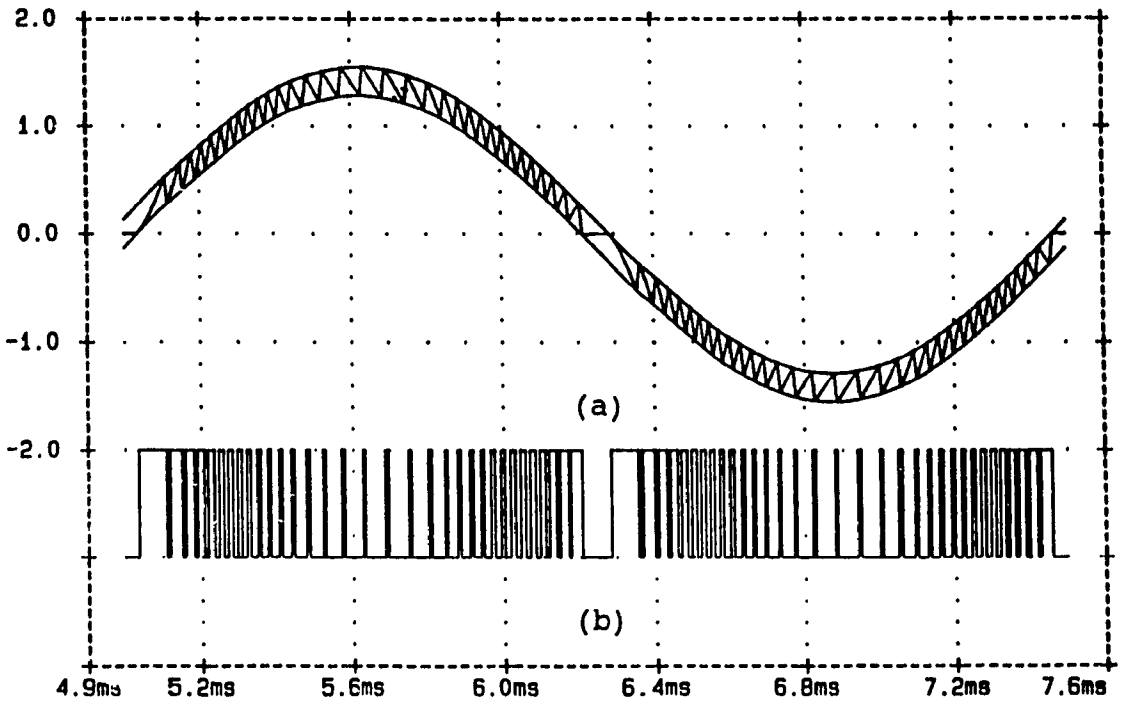

Fig. 2.10 Simulation results for one cycle of the AC input voltage (V_m = 1.414 p.u., V_o = 1.597 p.u., I_m=1.414 p.u., ΔI = 0.265 p.u., L = 0.094 p.u., and f_{IN}= 1 p.u.):

a) Line current within the hysteresis window;

b) Gating signal of the boost switch.

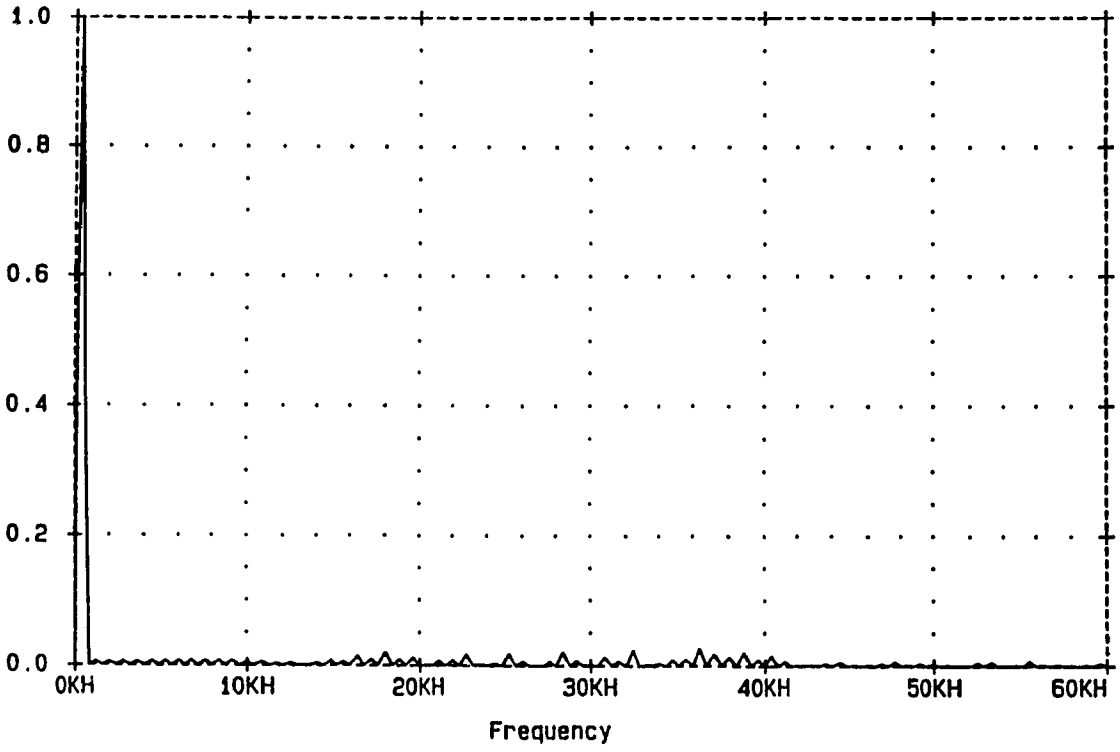

Fig. 2.11 Frequency spectrum of the input current (V_m = 1.414 p.u., V_o = 1.597 p.u., I_m = 1.414 p.u., ΔI = 0.265 p.u., L = 0.094 p.u., and f_{IN} = 1 p.u.).

cases, an LC - filter is usually used between the source and the front-end rectifier.

The values of L and C are normally found using the specified maximum allowable THD for the line current and the input voltage [21]. In this method, the current drawn by the rectifier is taken as a current source (Fig. 2.12). Then the AC voltage source is included in the equivalent circuit corresponding to the fundamental component of I_s and excluded from the equivalent circuit corresponding to other harmonics.

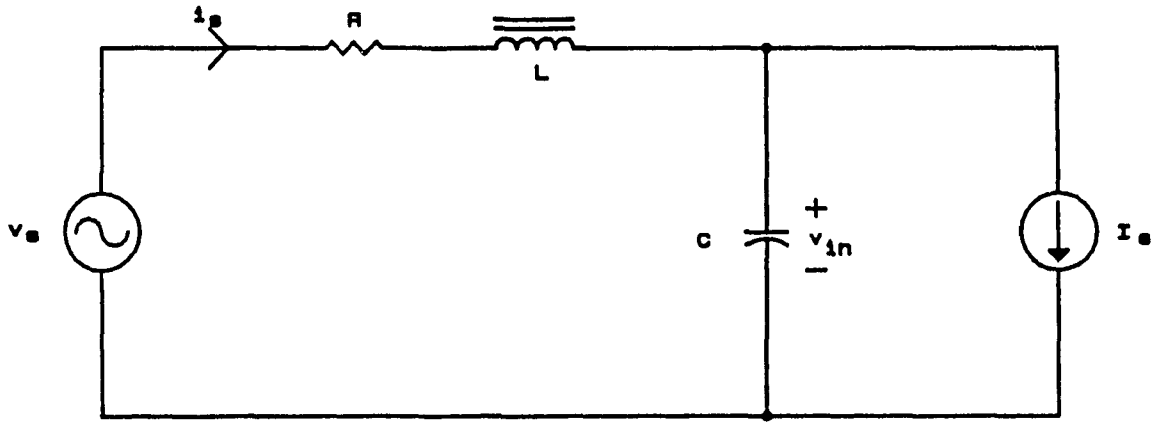

Fig. 2.12 Equivalent circuit of the AC source, input filter, and the front-end diode-rectifier input current waveshaper.

The values found for L and C by this method, determine the break frequency of the filter which is given by

$$f_b = \frac{1}{2\pi \sqrt{L\ C}} \tag{2.58}$$

Now, if in the frequency spectrum of the input current, there is no harmonic or no significant harmonic in the vicinity of f_b, the filter will work well; otherwise, the harmonics close to f_b, will be amplified because of the absence of damping or enough damping in the filter, resulting in a higher THD. Unfortunately, the latter is the case for the hysteresis control method, because the harmonics are spread over the whole frequency spectrum.

The above method was tried, taking a very low THD for the input voltage, and resulted in a THD of higher than 10% for the line current. The reason for this will become clear by looking at the characteristic equation of the LC-filter. The characteristic equation, considering a resistance R in series with the L (which can be the resistance of the inductor itself), will be:

$$s^2 + \frac{R}{L}\, s + \frac{1}{LC} = 0 \tag{2.59}$$

The standard form of the characteristic equation for a second order system is:

$$s^2 + 2\zeta\omega_n s + \omega_n^2 = 0 \tag{2.60}$$

where ω_n is the natural frequency and ζ the damping ratio of the system.

Comparing Eqns. (2.59) and (2.60), the damping ratio of the input filter can be obtained in terms of R, L, and C:

$$\zeta = \frac{R}{2}\sqrt{\frac{C}{L}} \qquad (2.61)$$

For the input voltage THD of 1% and line current THD of 5%, L and C were found to be:

$$L = 0.776 \text{ mH} = 0.041 \text{ p.u.;}$$

and

$$C = 2.834 \ \mu F = 0.342 \text{ p.u. .}$$

Therefore, for a damping ratio of $\zeta = 0.707$, R is found from Eqn. (2.61) to be:

$$R = 23.39 \ \Omega = 0.49 \text{ p.u.}$$

This amount of resistance cannot be inserted in the line in series with the inductor since it causes a considerable amount of line losses and voltage drop at the rectifier input.

At 60 Hz, the following typical relation exists between the inductance and the resistance of an inductor used for input filtering:

$$\frac{\omega L}{R} = \tan \theta \qquad (2.62)$$

where θ is an angle in the range of 80° to 85°. At 400 Hz, the right hand side of the above relation will be multiplied by a factor of 6.67. Therefore, for the inductance value found, the corresponding resistance is in the range:

$$(0.004 \ \Omega \cdot 0.008 \ \Omega) \text{ or } (8.1*10^{-5} \text{ p.u.} - 1.6*10^{-4} \text{ p.u.})$$

This means that the resistance associated with the filter inductor is not enough to provide the required damping. As mentioned earlier, insertion of an

additional resistance in series with the inductor, results in line losses as well as voltage drop at the rectifier input which is not desirable. Therefore, one has to restrict himself to the damping created by the resistance of the inductor.

Fig. 2.13 shows the variations of the magnitude of the input filter transfer function, i.e.,

$$T_F(s) = \frac{1}{LCs^2 + RCs + 1} \tag{2.63}$$

vs. frequency for the values obtained for R, L, and C. As seen, there is a considerable amplification around the break frequency of the filter over a rather wide range. This will amplify the current harmonics existing in this frequency band resulting in a higher THD than that found for when the input filter is not used.

2.7 Conclusions

The bang-bang hysteresis technique, is the most widely used current control technique for input current waveshaping purpose. It has the following special features:

- tight current regulation;
- instantaneous current control resulting in very fast response and high switch reliability; and
- simple control circuit.

However there are a few disadvantages which compromise the usefulness of the hysteresis current control technique. The most important drawbacks are:

- varying switching frequency within each half cycle of the AC input

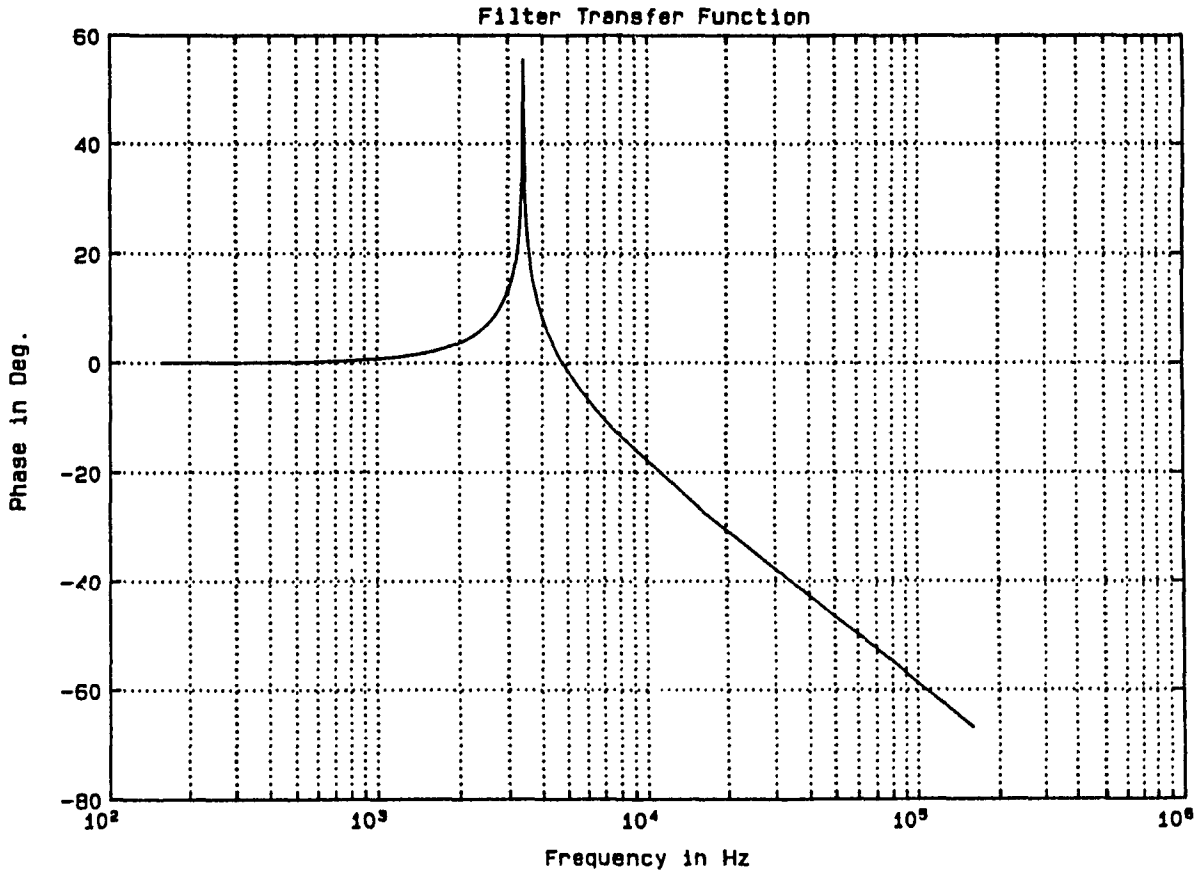

Fig. 2.13 Magnitude of the input filter transfer function vs. frequency.

voltage;

- varying average switching frequency as a result of circuit component value and/or parameter changes;
- possibility of the controlled current falling out of the hysteresis window (and thus temporary loss of control) because of unmatched current slope, reference and window size; and
- input current filtering very difficult to achieve because of the spread of the harmonics over the whole frequency spectrum.

CHAPTER 3

ERROR TRIANGULATION METHOD

3.1 Introduction

The bang-bang hysteresis control technique is simple, rugged, and offers instantaneous input current waveshaping. However, the switching frequency varies within each half cycle of the input AC voltage and also with component and parameter value changes, resulting in current harmonics spread over the whole frequency spectrum and making the input filter difficult to design. A novel input power factor correction method, which uses a closed loop active current waveshaping technique, will be introduced in this chapter as a remedy to the drawbacks of the hysteresis technique.

The novel feature of the proposed method (called "Error Triangulation Method") resides in the fact that nearly sinusoidal input currents are obtained at constant switching frequencies. Moreover, the method exhibits instantaneous current control which results in very fast response and increased switch reliability.

As in the previous chapter, a single-phase front-end diode-rectifier followed by a boost converter as the power processing unit will be considered in this chapter.

It will be shown that using the proposed control method, the design of the power circuit and the input filter (if necessary) becomes very easy. Furthermore, the control unit is simple to implement using analog circuitry.

Selected predicted system performance and design methods are verified experimentally on a 1 kVA laboratory prototype.

3.2 Principles of Operation

The basic circuit diagram of a single-phase front-end diode-rectifier followed by a step-up converter controlled using the proposed technique and used for the purpose of input current waveshaping is shown in Fig. 3.1.

When the boost switch is turned on, the inductor current builds up and energy is stored in the magnetic field of the inductor, while the boost diode is reverse biased and the capacitor supplies power to the load. This is the first mode of the operation of the power circuit (Fig. 2.2a). As soon as the boost switch is turned off, the power circuit changes mode (Fig. 2.2b) and the stored energy in the inductor, together with the energy coming from the AC input source, is pumped to the output circuitry (i.e., capacitor-load combination). This is mode 2 of the circuit. In mode 1,

$$|v_s| - L \frac{di_L}{dt} = 0 \tag{3.1}$$

while in mode 2,

$$|v_s| - L \frac{di_L}{dt} - v_o = 0 \tag{3.2}$$

If the switching frequency is much higher than the frequency of the line frequency, a quantity, "d'", defined to be the average off-duty ratio of the switch in one switching period, can be introduced. Therefore, Eqns. (3.1) and (3.2) can be combined:

$$|v_s| - L \frac{di_L}{dt} - d'v_o = 0 \tag{3.3}$$

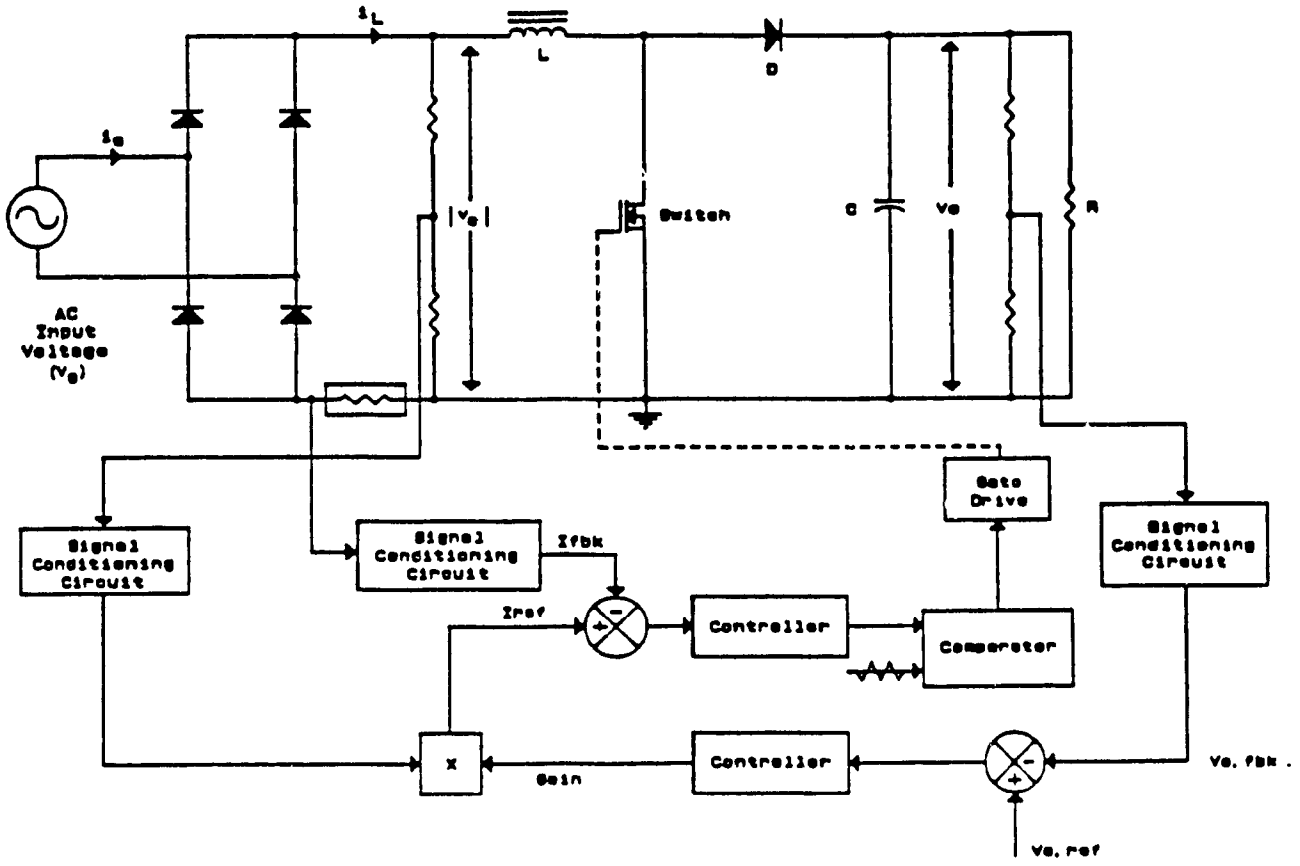

Fig. 3.1 A single-phase front-end diode-rectifier input-current waveshaping circuit controlled using the proposed technique.

In Eqn. (3.3), $|v_s|$ is the full-wave rectified sinusoidal input voltage, i_L the current through the inductor, and v_o the output voltage.

It is accepted that the output capacitor should be large enough to be able to supply power to the load when the switch is ON, and/or there is some temporary problem in the AC supply voltage or a sudden change in the load, without any appreciable dip in the output voltage (typical allowable dip or rise in the output voltage for a transient load change from 10% to 90% or vice versa, is 5%). Therefore, v_o is composed of a DC component (V_o) and a very small AC component at twice the AC line frequency (typical output voltage ripple% is less than 1%). Since the value of the capacitance is chosen to be large, the requirement of having enough stored energy in each half cycle of the AC input voltage, to take care of the difference between the time varying input power and the constant output power, is fulfilled.

In order to obtain a sinusoidal input current, in phase with the input voltage, the control unit should act in such a way that $|v_s|$ sees a resistive load equal to the ratio of $|v_s|$ and i_L. This is done by comparing the actual current passing through the inductor, with a current reference which is derived from $|v_s|$ and has an amplitude determined by the output voltage controller. The error is then triangulated to get the necessary gating signal to control the boost switch operation (Fig. 3.1).

The principles of operation can be explained from Fig. 3.2. On an average per switching period basis, $i_{L,ref}$ is compared with the center line through the $i_{L,fbk}$ waveform. If $i_{L,ref} > i_{L,fbk,ave}$, the average of the error waveform lies above zero line and when triangulated, results in higher than 50% on-duty ratio. In the case when $i_{L,ref} = i_{L,fbk,ave}$, the error is centered about zero level and the switch will be operated at 50% duty ratio.

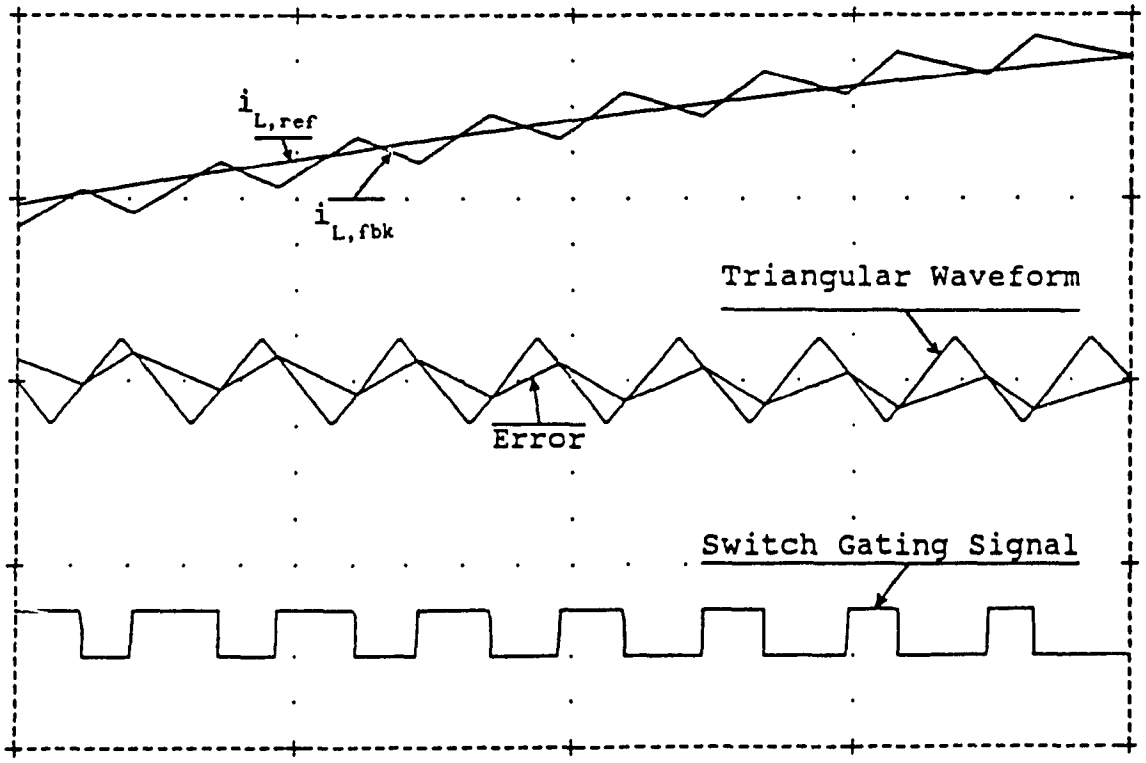

Fig. 3.2 Principles of operation of the proposed current waveshaping technique.

Finally, if $i_{L,ref} < i_{L,fbk}$, the average of the error waveform will lie below zero level and therefore, an on-duty ratio of lower than 50% results.

In this way, the error is forced to remain between the maximum and the minimum of the triangular waveform and as a result, the inductor current follows the reference closely. From what was said, it is clear that the smaller the peak-to-peak value of the triangular waveform, the closer the actual current to the reference.

In fact, the triangular waveform modulated on $i_{L,ref}$, provides an imaginary hysteresis window and the inductor current is always kept inside this window (Fig. 3.3).

3.2.1 Controller Options

The principles of operation of the proposed current waveshaping technique were explained assuming the current controller shown in Fig. 3.1 to be a proportional one. This is really one option for the current controller. In this case, there will be a band about each zero crossing of the input current, within which the current is in discontinuous mode (Fig. 3.9). This band which can be reduced in width by appropriate choice of circuit components and parameters, is produced due to the following:

A) In the beginning of each half cycle, the input voltage is small; thus the slope of the inductor current during the ON-state of the switch (whose maximum at each instant is determined by the value of $|v_s|$ and L) will be small. Therefore, the current cannot reach the reference when the first switching points should take place.

B) When the switch is turned off, the negative slope of the current is highest in the beginning of the half cycle, since $|v_s|$ is small. Therefore

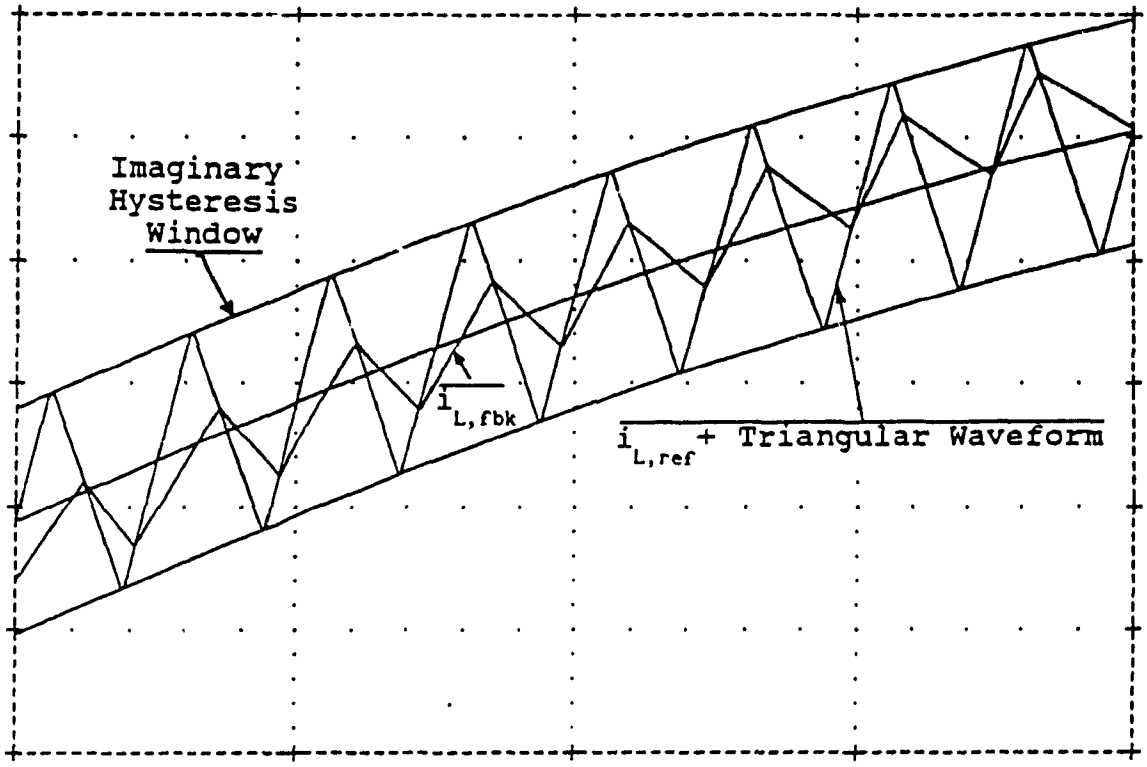

Fig. 3.3 The proposed active current waveshaping technique with its imaginary hysteresis window.

the difference between the output voltage (which is assumed to be constant for this analysis) and $|v_s|$, which is placed across the inductor, is high. Therefore, the current falls to zero before the next switching points can take place.

Also, in the case of a simple proportional controller, the real current will overshoot the current reference around the peak (Fig. 3.9). In fact, in this zone, the current touches the upper limit of the imaginary window introduced in Fig. 3.3.

In spite of both of the above shortcomings, which contribute to the distortion in the current waveform, in the form of low frequency harmonics, the results are quite satisfactory for the P-controller option.

Both problems mentioned above, i.e., a discontinuous current band around each zero crossing, and an overshoot around the peak, can be reduced by introducing an integration term in the current controller. In fact, by integrating the error, any difference between $i_{L,ref}$ and the center line through $i_{L,fbk}$ will be kept in the memory of the integrator until it is brought to zero (Fig. 3.11). The gain of the integrator should be chosen high, since the main purpose of using the integrator is to correct the low frequency component of the average value of error and not the instantaneous high frequency error.

From now on, the case of a simple proportional controller will be referred to as P-controller option and the case of a PI-controller, PI-controller option.

3.2.2 The Effect of the Amplitude of the Triangular Waveform

The total harmonic distortion (THD) of the line current is affected by

the amplitude of the triangular waveform. In fact, as the amplitude of the triangular waveform is increased, the THD of the input current will increase. This effect can be explained with reference to the fact that the error between $i_{L,ref}$ and $i_{L,fbk,ave}$, which is a measure of how closely the actual current follows the current reference, is kept within the band defined by the maximum and the minimum of the triangular waveform. Obviously, as the width of this band is increased, the average error is free to vary in a wider range and therefore a higher THD results because the actual current is following the reference less closely. The change in THD, as a result of a change in the amplitude of the triangular waveform, is most pronounced around the zero crossings and is reflected mainly as changes in low order harmonics of the input current waveform. Fig. 3.4 shows the effect of changes in the amplitude of the triangular waveform on the input current THD (taking into account only the first nine harmonics).

It is clear from Fig. 3.4 that THD is more affected by the changes in the amplitude of the triangular waveform in the P-controller option than in the PI-controller option. The reason is that in the case of PI-controller option, there is an additional control improving the tracking, which results in the reduction of the size of the low order harmonics and thus the changes in THD due to low order harmonics, produced by the changes in the amplitude of the triangular waveform.

It can be deduced that for best results, the amplitude of the triangular waveform should be kept as small as possible. The lower limit is determined by the maximum slope of the error which is in turn fixed by the maximum slope of the current (assuming that the switching frequency is much higher than the line frequency).

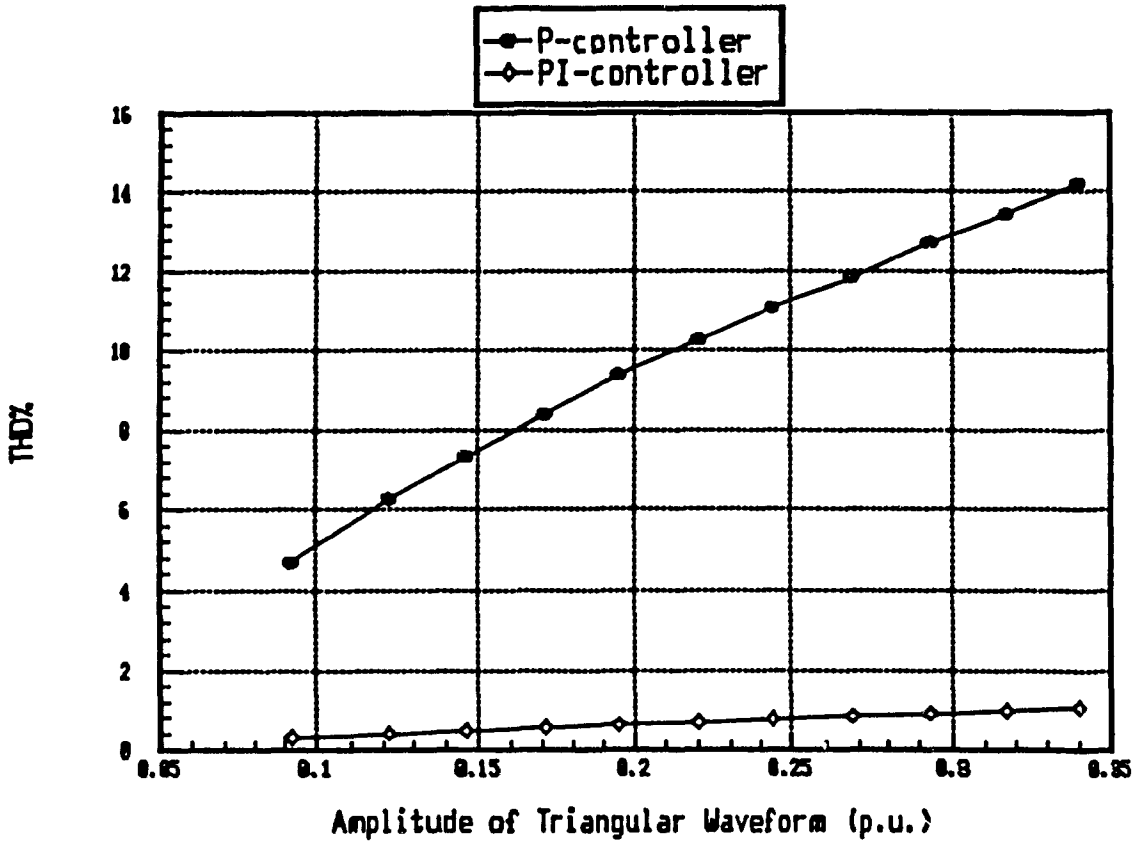

Fig. 3.4 Total harmonic distortion (THD) of the line current vs. the amplitude of the triangular waveform (V_m = 1.414 p.u., V_o = 1.913 p.u., I_m = 1.414 p.u., f_{in} = 1 p.u., f_{sw} = 666.67 p.u., and L = 0.026 p.u.).

The maximum slope of the inductor current during the ON-period of the switch occurs at the peaks of $|v_s|$ and can be found from Eqn. (2.1) to be:

$$m_{max.,ON} = \frac{V_m}{L}$$

while the maximum slope during the OFF-period happens at the zero crossings of $|v_s|$ and can be found from Eqn. (2.2) to be:

$$m_{max.,OFF} = -\frac{V_o}{L}$$

The triangular waveform should have at least the maximum slope of current during the ON-period of the switch for its rising edge, and the maximum slope during the OFF-period for its falling edge if no multiple switching points are expected. From the implementation point of view, a ramp waveform (Fig. 3.5a) with rising edge slope at least equal to the maximum slope of the current during the ON-period of the switch and very high falling edge slope is more practical. The triangular waveform (Fig.3.5b) generated by ordinary function generator chips is quite practical as well. In this case, the slope of the rising and falling edges are equal and should be chosen to be equal to the maximum slope of the current during OFF-period of the switch, i.e., V_o/L. In practice, since there are always stray resistances throughout the circuit (reducing the maximum slope of the current), and the period of time during which the slope of the falling current is greater than the slope of the rising current is very small, and during this period the current is discontinuous, no multiswitching will therefore happen if the slope of the triangular waveform is taken to be equal to the maximum slope of the current during the ON-period of the switch.

Fig. 3.5 Typical ramp and triangular waveforms.

For any desired switching frequency, the minimum amplitude of the triangular waveform can then be found using the maximum slope of the current during the ON-period of the switch. Reducing the amplitude below this value, will cause multiswitching and disturb the operation of the switch. (In fact, as the amplitude tends to zero, the switching operation is changed to linear operation).

It is worth noting that since the switching frequency is usually chosen to be very high compared to the line frequency, the effect of any phase or frequency drift in the triangular waveform is negligible; thus in practice, no synchronization is needed for the triangular waveform with respect to the input voltage. Also, the frequency of switching does not need to be an integer multiple of the line frequency.

3.2.3 The Range of Current Control

Since there is an output voltage controller in the system of Fig. 3.1 which is keeping the output voltage at the desired level, the inductor current, and as a result the line current can be reduced to zero by keeping the boost switch in OFF-state for a long enough period of time. This happens

when there is a sudden rise in the output voltage resulting from an open circuit at the output terminals.

The other extreme case is when there is a short circuit at the output terminals. In this case, the output voltage controller dictates a very high on-duty ratio to the switch. This results in a very high input current. This current is limited by the values of v_s and the resistances and inductances in the loop containing v_s, the line impedance, the diode rectifier, the boost inductor and the boost switch. This limit corresponds to an on-duty ratio equal to 1. For higher $i_{L,ref}$ values dictated by the output voltage controller, the actual current will be independent of $i_{L,ref}$. But, in fact, this limit can never be reached, because the ratings of the components of the power circuit and the saturation levels of the components in the control circuit are well below this level. To protect the circuit against overcurrent and short circuit, a proper fuse is necessary in the path of the input current.

Furthermore, to limit the in-rush current at start-up, a current limiting resistor can be placed in series with the boost inductor, which will be bypassed by a contactor or a thyristor subsequent to the initial transient. The problem with the inrush current can also be solved by ramping the output voltage reference.

3.3 Converter Analysis

Fig. 3.6 shows the inductor current and the current reference for a few switching periods.

It is assumed that the switching frequency is much higher than the line frequency and the actual current waveform follows the current reference

exactly (which can be realized to a very good approximation using PI-controller option). Under these assumptions, ΔI can be defined to be the peak-to-peak ripple current during one switching period. Of course, ΔI is not a fixed value as it was in the case of hysteresis control technique, and will vary during each half cycle of the AC input voltage. Eqns. (2.1) to (2.17) are valid for the case of error triangulation method.

Since in this method, the switching frequency is kept constant, and ΔI is varying, it is better to modify Eqn. (2.17) to the following form:

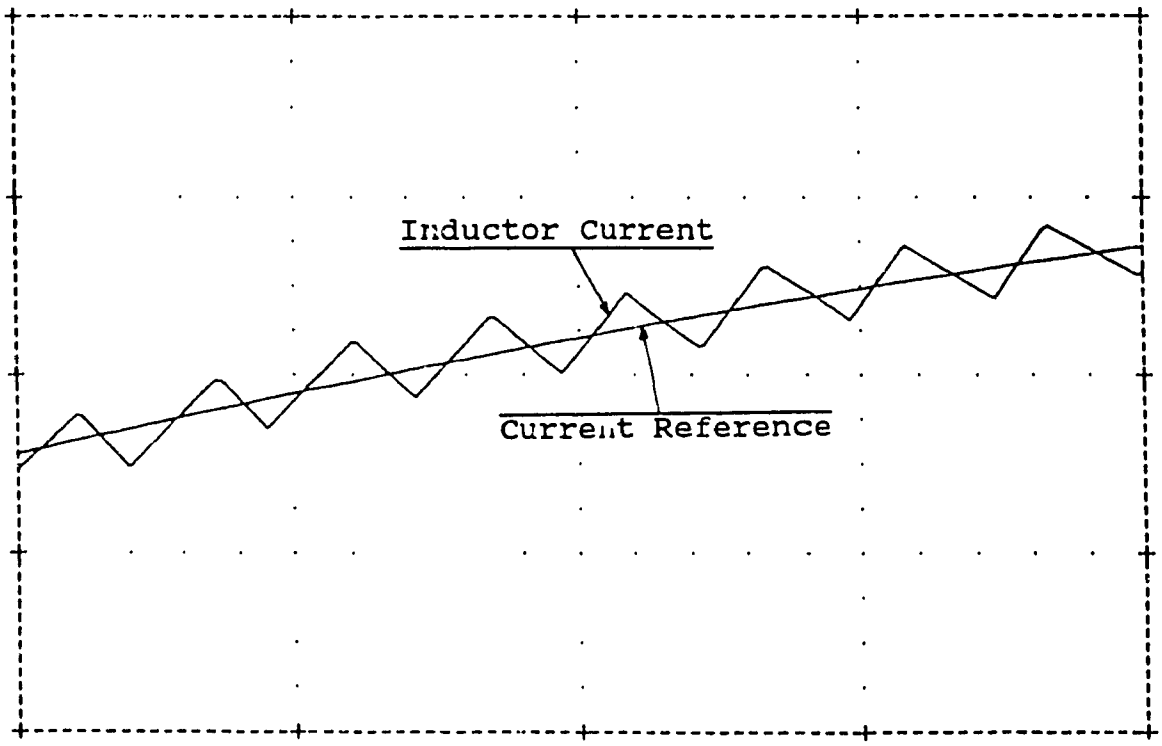

Fig. 3.6 Inductor current and the current reference.

$$\Delta I = \frac{(V_m \sin \omega t - \omega L I_m \cos \omega t)\left[V_o - (V_m \sin \omega t - \omega L I_m \cos \omega t)\right]}{L\, f_{sw}\, V_o} \qquad (3.4)$$

The variations of the current ripple (ΔI) vs. time during a full cycle of the AC input voltage will be the same as that shown in Fig. 2.6, if the values corresponding to the vertical axis are scaled by the factor:

$$\frac{(\Delta I)_{hysteresis}}{f_{sw,error\ triangulation}}$$

and the vertical axis label is changed to ΔI. The maximum occurs approximately at $\omega t = \sin^{-1}(V_o / 2V_m)$. Eqn. (3.4) can be used to design L for a specified maximum current ripple.

The average current ripple in a half cycle of the AC input voltage can be derived from Eqn. (2.18) to be

$$(\Delta I)_{ave} = \frac{4V_o V_m - \pi(\omega^2 L^2 I_m^2 + V_m^2)}{2\pi\, L\, f_{sw}\, V_o} \qquad (3.5)$$

As seen, the average current ripple is almost insensitive to the variations of the amplitude of the current reference (because of the factor L^2 which is usually very small), but is affected by the changes in V_m, V_o, L, and f_{sw}.

Assuming V_m and L to be constant values, the effects of V_o and f_{sw} on the average current ripple can be investigated by looking at Figs. 2.7 and 2.8. In Fig. 2.7, the label of the vertical axis should be changed to $(\Delta I)_{ave}$ and the values corresponding to the vertical axis scaled by a factor. Also, in Fig. 2.8, the label of the vertical and horizontal axes should be changed to

$(\Delta I)_{ave}$ and f_{sw} respectively and the values corresponding to the two axes scaled by appropriate factors.

It is clear that as the output voltage is increased, the average current ripple will increase as well, and vice versa. This effect can be sensed during the output voltage transients resulting from load changes.

Furthermore, it is obvious that as the switching frequency is increased, the average current ripple will be decreased, and vice versa. This means that the higher the switching frequency, the more closely the actual current follows the reference.

Before closing this section, it is useful to look at the variations of the on-duty ratio of the switch within a half cycle of the AC input voltage. From Eqn. 3.3,

$$d' = \frac{|v_s| - L\dfrac{di_L}{dt}}{V_o} \tag{3.6}$$

If "d" is defined to be the average on-duty ratio of the switch in one switching period,then

$$d = 1 - d' \tag{3.7}$$

and Eqns. (3.6) and (3.7) yield

$$d = \frac{V_o - (|v_s| - L\dfrac{di_L}{dt})}{V_o} \tag{3.8}$$

Under the same assumptions as were made in the beginning of this section, Eqn. (3.8) can be changed to

$$d = \frac{V_o - (V_m \sin \omega t - \omega L I_m \cos \omega t)}{V_o} \qquad (3.9)$$

Fig. 3.7 shows the variations of "d" during one complete cycle of the AC input voltage. It indicates that the maximum on-duty ratio of the switch occurs at the zero crossings of the AC input voltage, while its minimum is located at $\omega t = 90^{\circ}$ where the AC input voltage has reached its peak. The same pattern will be repeated in every half cycle of the AC input voltage.

The average of the on-duty ratio in a half cycle of the AC input voltage ($\overline{D}$) is controlled by the current reference which is in turn controlled by the output voltage controller. In fact, a higher current reference value which is a result of a higher output voltage demand, will result in a higher $\overline{D}$, and vice versa.

3.4 Ratings of the Converter Components

The ratings will be the same as those found in section 2.4.

3.5 Design Procedures

The complete design includes the design of the power circuit, and the current regulator. The size of the boost inductor and the output capacitor are found using the corresponding design specifications. Then the current regulator is designed accordingly.

3.5.1 Design of Power circuit

3.5.1.1 Design of L

To start with, it will be very helpful to relate the input current THD%

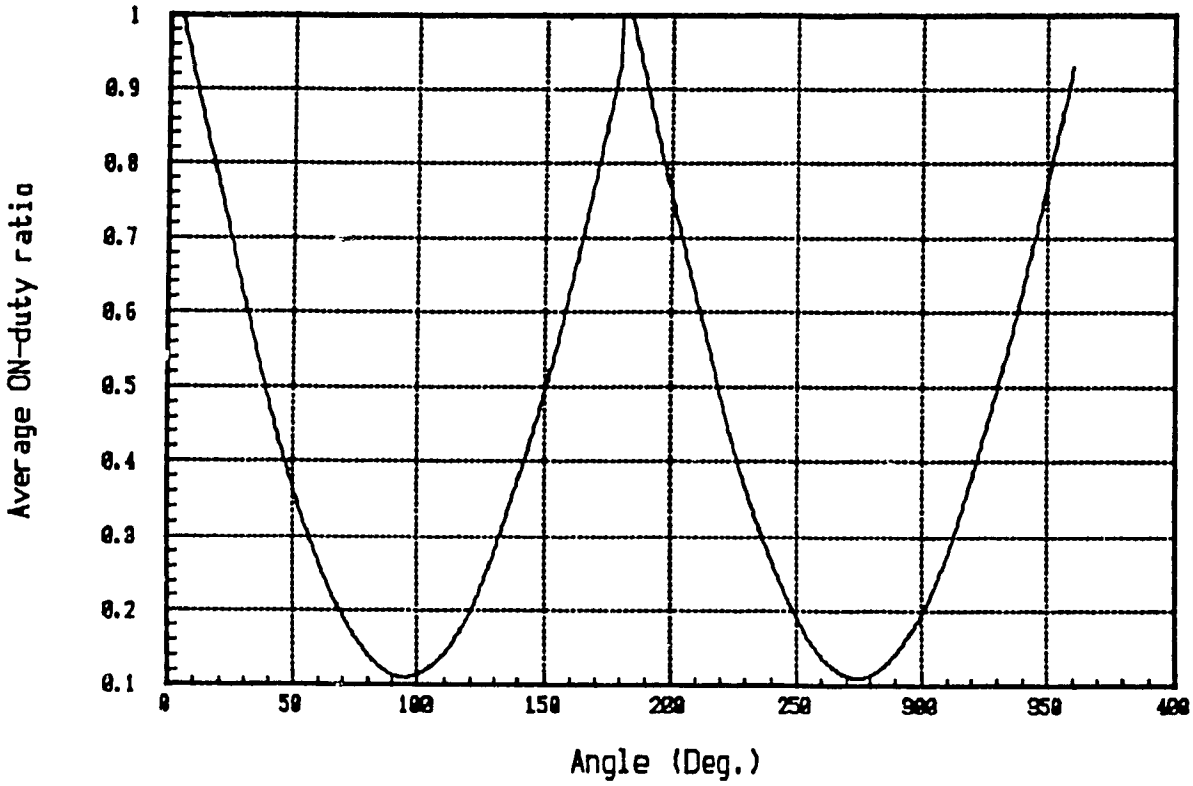

Fig. 3.7 Variations of the average on-duty ratio of the boost switch during one cycle of the AC input voltage (V_m = 1.414 p.u., V_o = 1.597 p.u., I_m = 4.384 p.u., f_{IN} = 1 p.u., and L = 0.026 p.u.).

to the input current percent ripple, defined by

$$\text{ripple\%} \triangleq \frac{\text{rms value of fundamental component of ripple current}}{\text{rms value of current reference}}(100) \tag{3.10}$$

THD% is defined by

$$\text{THD\%} = \frac{\left[\sum_{n=2} I^2_{n,rms}\right]^{1/2}}{I_{1,rms}}(100) \tag{3.11}$$

If the input current is very close to sinusoidal (which can be realized using PI-controller option), then there will be almost no contribution to the THD from low order harmonics in the input current. Then, to a very good approximation, THD in the input current can be assumed to be caused by the harmonics generated by switching, among which the harmonic at the switching frequency is of the greatest significance. Based on the above facts, Eqn. (3.11) can be changed to:

$$\text{THD\%} \cong \frac{I_{ns,rms}}{I_{1,rms}}(100) \tag{3.12}$$

where n_s is the order of the current harmonic at the switching frequency. Under these conditions, the numerators and the denominators of Eqns. (3.10) and (3.11) are almost equal and therefore,

$$\text{ripple\%} \cong \text{THD\%} \tag{3.13}$$

Using the fact that maximum allowable THD% corresponds to maximum allowable ripple%, and knowing that maximum current ripple occurs when the duty cycle of the switch is 50%, the following relation results:

$$(THD\%)_{max,allowable} = \frac{I_{lr,rms}\text{ , at 50\% duty cycle}}{I_{ref,rms}} \qquad (3.14)$$

where $I_{lr,rms}$ and $I_{ref,rms}$ are the RMS value of the fundamental component of the ripple current and the RMS value of the current reference, respectively.

Given maximum allowable THD% and the RMS value of the current reference, the RMS value of the fundamental component of the ripple current at 50% duty cycle can be found. From now on, there are two different methods to reach the desired value of the boost inductor.

The first method is to find $(\Delta I)_{max}$ using the RMS value of the fundamental component of the ripple current at 50% duty cycle and then put it in Eqn. (3.4). Then, this Equation and a second one which can be obtained by equating the derivative with respect to time of Eqn. (3.4) to zero, yield the proper value for L. This is almost the same method as was used to find L in the case of hysteresis control; but, in this case, there is no need to impose another constraint on the value of L, since the slope of the triangular waveform will be found according to the maximum value of the slope of the current which is in turn determined by the value of L.

The second method is based on the fact that the inductor current is controlled by two voltages; one is the rectified sinusoidal input voltage which is applied to one side of the inductor, and the other one is the voltage across the switch which varies between zero and V_o due to switching and is applied to the other side of the inductor. The voltage that contributes to the ripple, is the voltage across the switch. In other words, it can be said that the ripple current is produced by an equivalent square wave of amplitude V_0 / 2 and frequency equal to the switching frequency. At

50% duty cycle which corresponds to the maximum ripple in the input current, and based on the above facts, the output voltage (V_o), the switching frequency (f_{sw}), the inductance value (L), and the RMS value of the fundamental component of the ripple current ($I_{lr,rms}$), are related through the following relation

$$\left(\frac{V_o}{2}\right)\left(\frac{4}{\pi\sqrt{2}}\right) = (2\pi f_{sw} L)\, I_{lr,rms} \qquad (3.15)$$

Note that the left hand side of Eqn. (3.14) is the RMS value of the fundamental component of the switched voltage at 50% duty cycle.

3.5.1.2 Design of C

The procedure for the design of the output capacitor is exactly the same as that explained in section 2.5.2.

3.5.2 Current Regulator Design

The design of the current regulator includes the choice of the amplitude of the triangular waveform, with which the error signal is to be compared, and the integral term, in the case of PI-controller option.

The minimum value for the amplitude of the triangular waveform can be readily found from the maximum value of v_s, the value of L, and the specified switching frequency. The maximum slope of the inductor current is:

$$m_{max} = \frac{v_{s,peak}}{L} = \frac{v_m}{L} \qquad (3.16)$$

Given the switching frequency, the amplitude of the triangular waveform corresponding to the above slope of current is found using the following

equation:

$$A_{min} = (\frac{T_{sw}}{4})(m_{max}) = \frac{V_m}{4f_{sw}L} \tag{3.17}$$

It is worth noting that A_{min} will be scaled by the same factor as i_L in the control circuit.

The integral term of the PI-controller is chosen based on the criterion that its time constant should be larger than one switching period, in order for the controller to correct only the low frequency error.

The transfer function of a PI-controller can be written as:

$$T_{PI}(s) = K_P + \frac{K_I}{s} \tag{3.18}$$

where K_P and K_I are the proportional and integral coefficients of the controller. This can be compared with the transfer function of a simple PI-controller realized by an Op. Amp. circuit (Fig. 3.8) to obtain the proper component values.

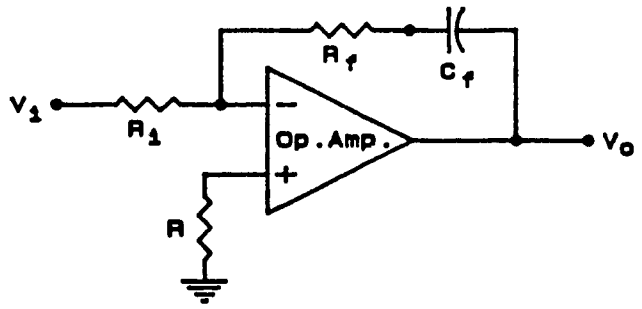

Fig. 3.8 A simple PI-controller circuit.

The transfer function of the above PI-controller circuit is:

$$\frac{V_o}{V_1}(s) = \frac{R_f}{R_1} + \frac{1}{R_1 C_f s} \tag{3.19}$$

Comparison of Eqns. (3.18) and (3.19) yields:

$$K_P = \frac{R_f}{R_1}$$

and

$$K_I = \frac{1}{R_1 C_f} \tag{3.20}$$

The proportional factor is 1 for both P-controller and PI-controller options. Therefore,

$$R_f = R_1$$

The integral factor is the inverse of the time constant of the PI-controller, as seen from Eqn. (3.20), and since the time constant should be larger than one switching period, K_I has to be less than the switching frequency. The highest sensitivity of the PI-controller is obtained for:

$$K_I = \frac{1}{R_1 C_f} = \frac{1}{T_{sw}} = f_{sw} \tag{3.21}$$

But this calls for a very high K_I lowering the speed of response of the current regulator. On the other hand, K_I can not be chosen very small, since in that case the time constant of the PI-controller becomes comparable with the period of the line current and the controller will not respond to the low frequency error. Therefore, a compromise should be made between the speed of response and the accuracy of tracking. For K_I values in the range (0.5 f_{sw} - f_{sw}), satisfactory results can be obtained.

3.6 Design Example

The design specifications and the base values are the same as those given in section 2.5, except for the desired switching frequency:

$$\text{Switching Frequency } (f_{sw}) = \text{constant} = 40 \text{ kHz.}$$

As before, given the design specifications and base values, and assuming the converter to be lossiess,

$$i_s = 1 \text{ p.u.;}$$

$$V_o = 1.91 \text{ p.u.;}$$

and the load resistance,

$$R_L = 3.65 \text{ p.u. .}$$

3.6.1 Design of Power Circuit

3.6.1 1 Design of L

By Eqn. (3.14) and from the design specifications,

$$I_{lr,rms} = 0.05 \text{ p.u. .}$$

Therefore, L is found from Eqn. (3.15) to be

$$L = 0.9 \text{ mH} = 0.026 \text{ p.u. .}$$

3.6.1.2 Design of C

The value of C is exactly the same as that found in section 2.5.2.

3.6.2 Design of Current Regulator

The maximum slope of the inductor current can be obtained from Eqn. (3.16):

$$m_{max} = \frac{V_m}{L} = \frac{(\sqrt{2})(115)}{0.0009} = 180.71 \text{ kA/s} .$$

For f_{sw} = 40 kHz, the amplitude of the triangular waveform which corresponds to the above slope of current is found from Eqn. (3.17):

$$A_{min} = (\frac{25}{4})(10^{-6})(180710) = 1.13 \text{ A} = 0.13 \text{ p.u.} .$$

The proportional factor for both P and PI- controller options is 1 as mentioned in section 3.5.2. The integral factor for the PI-controller is taken to be equal to the switching frequency, i.e., 40 kHz.

3.7 Output Voltage Control Loop

3.7.1. Steady State Analysis

Since the break frequency of the output filter is very low, one can say that the output voltage is controlled only by the average value of the on-duty ratio of the switch in a half cycle of the AC input voltage, $\bar{D}$:

$$V_o = \frac{|v_s|_{,ave}}{1 - \bar{D}} = \frac{2}{\Pi} V_m \frac{1}{1 - \bar{D}} \qquad (3.22)$$

Also, the boost diode and the inductor currents can be related as follows:

$$i_D = d' i_L \qquad (3.23)$$

Combining Eqns. (3.22) and (3.23), and assuming that $i_L = I_m |\sin \omega t|$, the average of the diode current over a half cycle of the AC input voltage is found to be

$$\bar{I}_D = \frac{V_m I_m}{2V_o} \tag{3.24}$$

Also, the average of the inductor current over a half cycle of the AC input voltage is

$$\bar{I}_L = \frac{2}{\pi} I_m \tag{3.25}$$

Therefore, Eqns. (3.22), (3.24), and (3.25) yield

$$\bar{I}_D = \frac{\pi^2}{8} (1 - \bar{D})\bar{I}_L \tag{3.26}$$

But,

$$\bar{I}_D \cong \frac{V_o}{R_L} \tag{3.27}$$

Therefore, Eqns. (3.22), (3.26), and (3.27) give

$$\bar{I}_L = \frac{16V_m}{\pi^3 R_L (1 - \bar{D})^2} \tag{3.28}$$

Knowing that $i_{L,ref}$ and i_L are related by a constant,

$$i_L = K_1 i_{L,ref} \tag{3.29}$$

the following relation can be derived using Eqns. (3.28) and (3.29):

$$\bar{D} = 1 - \frac{2}{\pi} \left(\frac{2V_m}{K_1 R_L i_{L,ref,peak}}\right)^{1/2} \tag{3.30}$$

Eqns. (3.22) and (3.30) yield

$$V_o = \left(\frac{K_1 R_L}{2} V_m i_{L,ref,peak}\right)^{1/2} \tag{3.31}$$

Knowing that $i_{L,ref}$ is obtained by scaling a sample of $|v_s|$, ($|K_2|v_s|$), using the output of the voltage controller, e,

$$V_o = \left(\frac{K_1 K_2}{2} R_L V_m^2 e\right)^{1/2} \tag{3.32}$$

or

$$V_o = K\sqrt{e} \tag{3.33}$$

where

$$K = \left(\frac{K_1 K_2}{2} R_L V_m^2\right)^{1/2} \tag{3.34}$$

The above equation is nonlinear and is therefore linearized around the operating point defined by E and $\overline{V}_o$:

$$\text{DC:} \quad \overline{V}_o = K\sqrt{E} \tag{3.35}$$

$$\text{AC:} \quad \hat{V}_o = \frac{1}{2} K E^{-1/2} \hat{e} \tag{3.36}$$

3.7.2. Voltage Controller

Since the voltage loop is working at a frequency below the output filter corner frequency, the phase shift of the converter-filter combination is minimal and a simple PI-controller will allow the compensation of the voltage loop.

In the experimental set-up, the linearization was performed around 220 V which corresponds to E = 0.98 (K = 223.61). The stability is achieved around the operating point and assumes small variations. The transient behavior of the system can be significantly improved by adding a feedforward signal from the load current to the output of the voltage controller.

3.8 Simulation Results

For the same reason as was mentioned in section 2.6, i.e., the limited size of the data file generated by the simulation program that can be handled

by the postprocessor, the design specifications and base values are changed to those given in section 2.6, except for the desired switching frequency:

$$\text{Switching Frequency } (f_{sw}) = \text{constant} = 40 \text{ kHz.}$$

As a result, as previously,

$$i_s = 1 \text{ p.u.;}$$

$$V_o = 1.597 \text{ p.u.;}$$

and

$$R_L = 122.53\ \Omega = 2.55 \text{ p.u.} .$$

Now, following the procedures for the design of L and C explained in sections 3.5.1 and 3.5.2, the following values are found for L and C:

$$L = 2.\ 748 \text{ mH} = 0.144 \text{ p.u.;}$$

and

$$C = 162.4\ \mu F = 19.6 \text{ p.u.} .$$

Also, the maximum slope of the current is found to be

$$m_{max} = 112809.31 \text{ A/s} .$$

Therefore, the amplitude of the triangular waveform corresponding to the above slope of current will be

$$A_{min} = 0.705 \text{ A} = 0.155 \text{ p.u.} .$$

Fig. 3.9 shows the simulation results for one complete cycle of the AC input voltage, for the case of P-controller option. The frequency spectrum of the input current for the case of P-controller option is shown in Fig. 3.10.

The THD in the input current is found to be 6.37% . The THD is larger than 5%, since in the design of L, we assumed to have only high frequency (in the order of switching frequency) harmonics in the current, while in P-controller option, there are low order harmonics as well as high order ones, as can be seen from Fig. 3.10 .

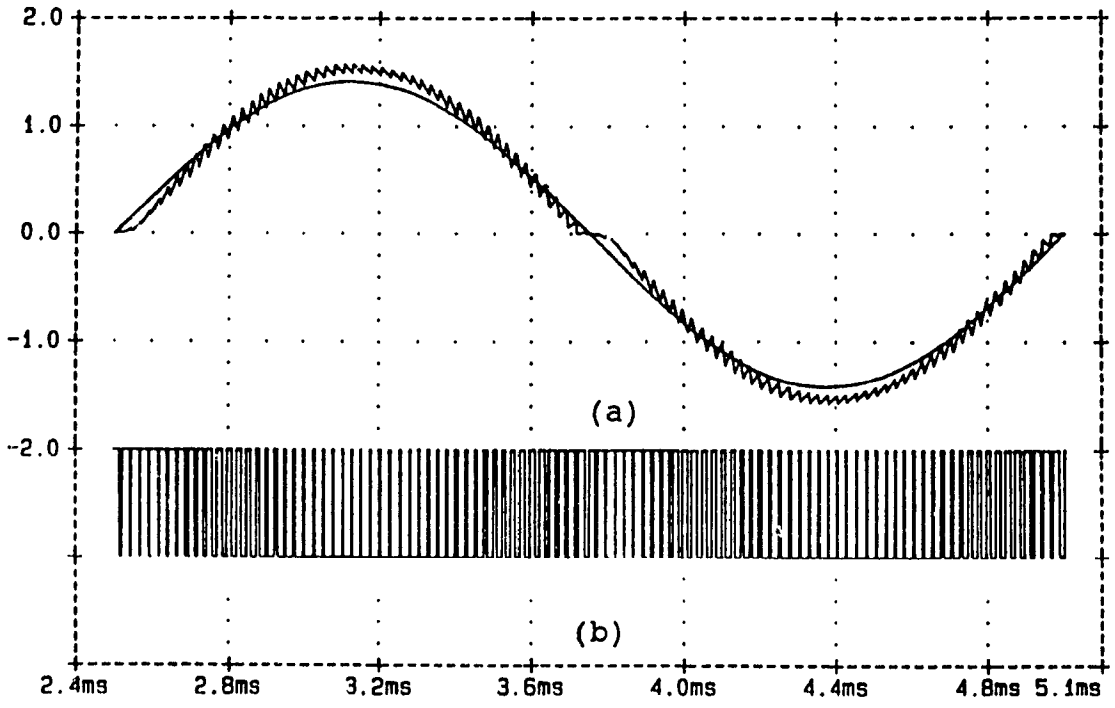

Fig. 3.9 Simulation results for one cycle of the AC input voltage (P-controller option), (V_m = 1.414 p.u., V_o = 1.597 p.u., f_{line} = 1 p.u., I_m = 1.414 p.u., and L = 0.144 p.u.):

a) Line current and the current reference;

b) Gating signal of the boost switch.

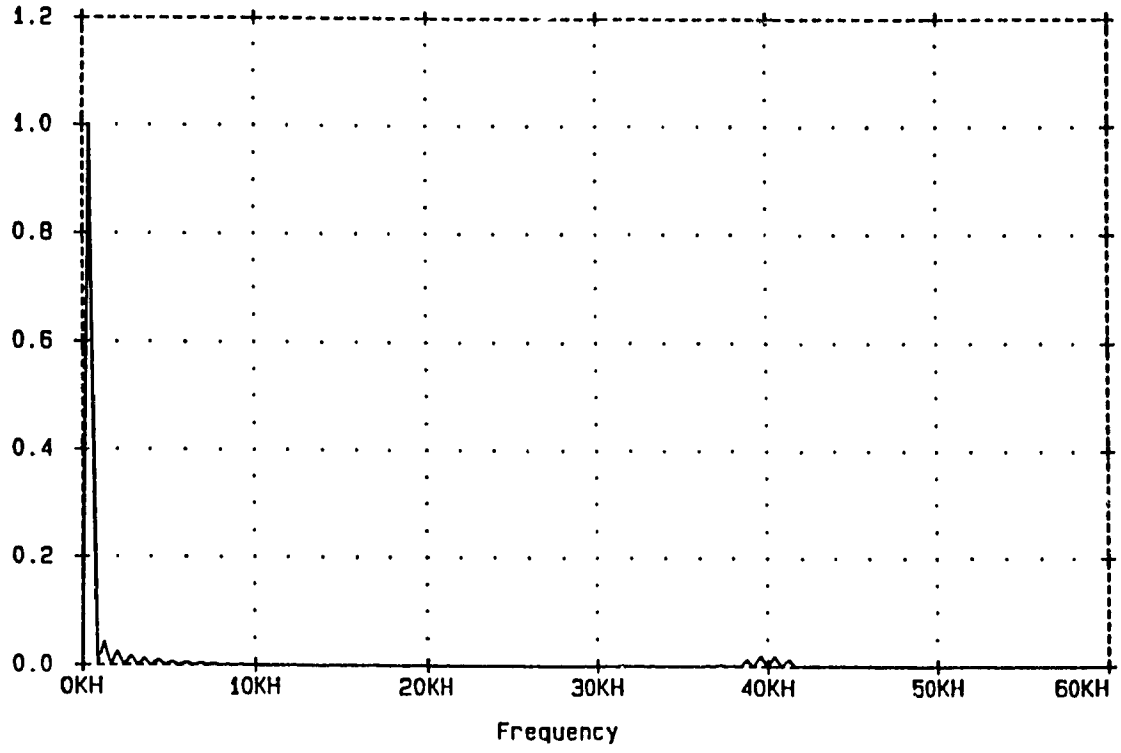

Fig.3.10 Frequency spectrum of the input current (P-controller option), (V_m = 1.414 p.u., V_o = 1.597 p.u., f_{line} = 1 p.u., I_m = 1.414 p.u., and L = 0.144 p.u.)

To take care of the THD in excess of 5%, an input filter should be used. In the case of "Error Triangulation Method", because of having constant switching frequency, there is an almost harmonic-free zone between the low order harmonics and high order ones; therefore, an LC filter can be easily designed to reduce the input current THD to 5% .

Fig. 3.11 shows the simulation results for one complete cycle of the AC input voltage, for the case of PI-controller option. The frequency spectrum of the input current, for the case of PI-controller option, is shown in Fig. 3.12 .

The THD in the input current is found to be 5.07% . The THD is almost equal to 5% . The small difference is due to the fact that the input current is not completely free of low order harmonics as can be seen from Fig. 3.12. Practically, no filter is necessary at the input of the front-end diode rectifier. In case the limitation on the THD of the input current is so strict that no THD greater than 5% can be accepted, the design of the filter is straight forward and very easy as it was for P-controller option.

3.9 Experimental Results

A 1 kVA converter using the parameters given in the design example (section 3.6) was set up in the laboratory. The waveforms of the input current and AC input voltage obtained for both P-controller and PI-controller options are shown in Figs. 3.13a and 3.14a, respectively. Also, the frequency spectrum of the input current for both control options are shown in Figs. 3.13b and 3.14b, respectively.

The experimental results are found to be consistent with the simulation results. Also, the voltage loop operates properly for small variations in the

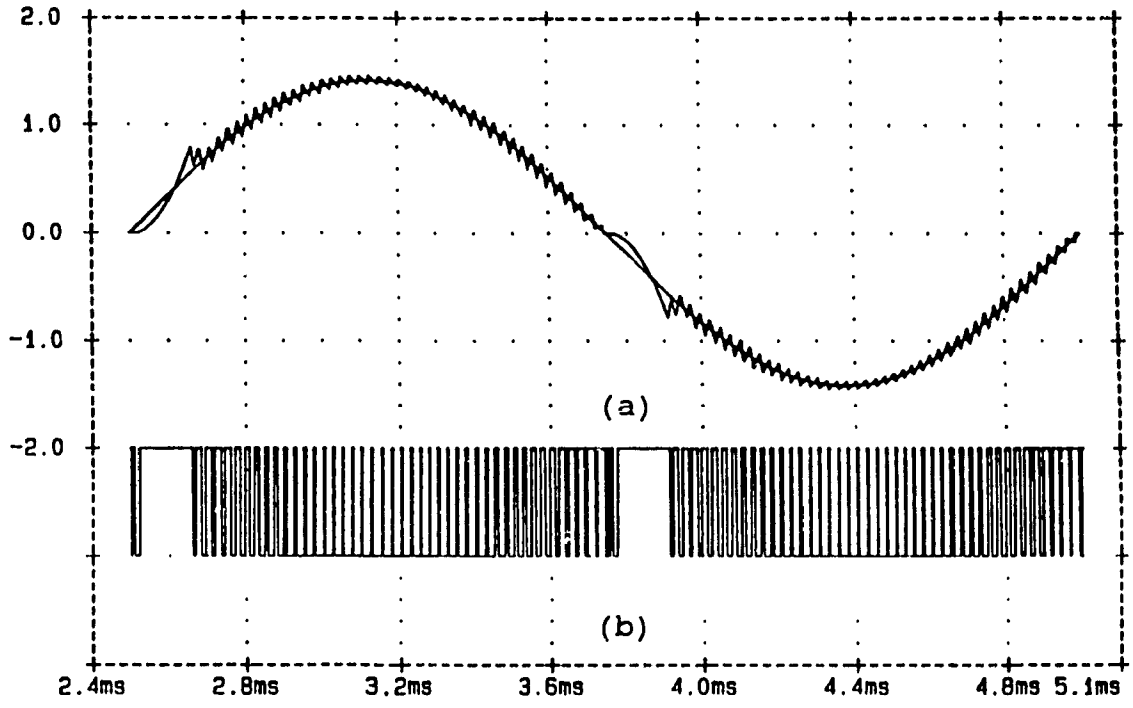

Fig. 3.11 Simulation results for one cycle of the AC input voltage (PI - controller option), (V_m = 1.414 p.u., V_o = 1.597 p.u., f_{line} = 1 p.u., I_m = 1.414 p.u., and L = 0.144 p.u.)

a) Line current and the current reference;

b) Gating signal of the boost switch.

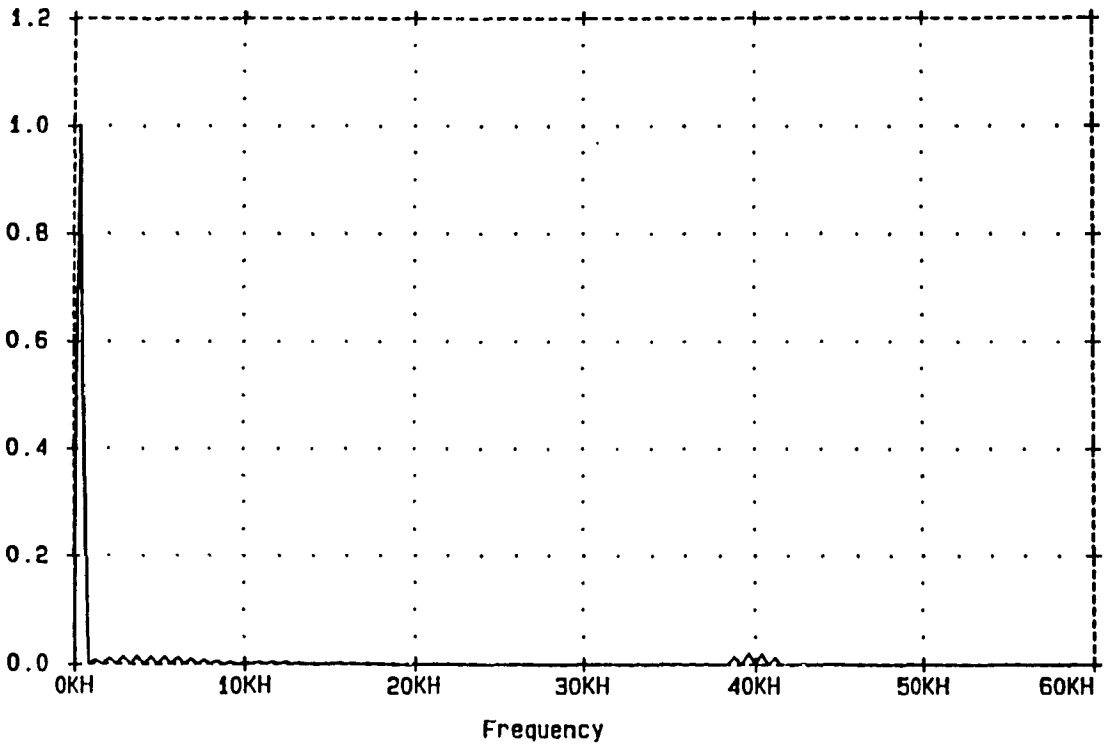

Fig. 3.12 Frequency spectrum of the input current (PI-controller option), (V_m = 1.414 p.u., V_o = 1.597 p.u., f_{line} = 1 p.u. , I_m = 1.414 p.u., and L = 0.144 p.u.)

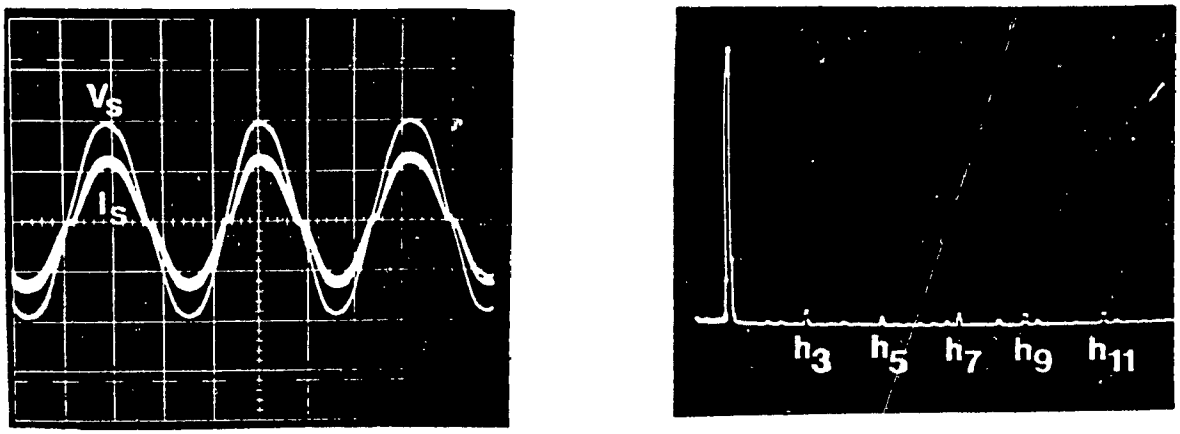

(a) (b)

Fig. 3.13 Experimental results for P-controller option:

a) Input current and voltage waveforms; t=5 ms/div, current = 10 A/div, and voltage = 84 V/div .

b) Frequency spectrum of the input current

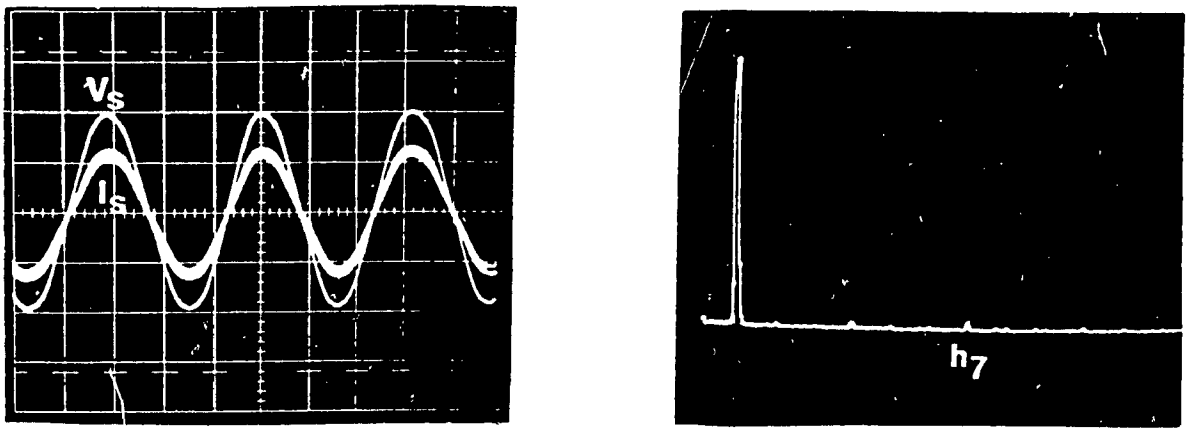

(a) (b)

Fig. 3.14 Experimental results for PI-controller option:

a) Input current and voltage waveforms; t=5 ms/div, current = 10 A/div, and voltage = 84 V/div .

b) Frequency spectrum of the input current.

load and input voltage.

3.10 Conclusions

The error triangulation current control method provides instantaneous waveshaping , as the hysteresis control method. However, in this method, the switching frequency is constant and the harmonic distortion lower. Its features can be summarized as follows:

- fixed switching frequency;
- instantaneous current control resulting in very fast response and switch reliability;
- controllable current ripple amplitude by choice of appropriate inductance value, and triangular waveform amplitude and frequency.
- no need for input filtering in the case of PI-controller option;
- easy input filter design, if necessary (P-controller option); and
- simple control circuit implementation.

CHAPTER 4

PREDICTIVE METHODS

4.1 Introduction

The "Error Triangulation Method", presented in chapter 3, offers a number of advantages, among which, constant switching frequency, low harmonic distortion, and simple hardware implementation. However, the above method requires a current sensor and produces some distortion around the zero crossings of the current. Programmed techniques may be used to overcome these problems.

Two programmed methods for shaping the input current and controlling the input power factor of front-end diode-rectifiers are introduced in this chapter.

Both methods yield nearly sinusoidal input currents at constant switching frequency. Moreover, instantaneous current control is achieved which results in very fast response and increased switch reliability. The proposed methods are also compatible with microprocessor-based converter controls. The second method has the added advantage of eliminating the need for input current sensing.

As in chapters 2 and 3, a single-phase front-end diode-rectifier followed by a boost converter, as the power processing unit, will be considered in this chapter.

It will be shown that using the proposed control methods, the design of

the power circuit becomes very easy. Also, no input filter is necessary, since the desired input current THD can be achieved simply by proper design of the power circuit components. However, the design and adjustment of the control unit needs careful considerations.

Design data and predicted system performance are verified experimentally on a 1 kVA laboratory prototype.

4.2 Principles of Operation

4.2.1. Method 1

The basic circuit diagram of a single-phase front-end diode-rectifier plus a boost converter controlled by the first proposed control technique and used for the purpose of input current waveshaping is shown in Fig. 4.1 .

Required is a switching function for the boost switch, which forces the current through the inductor, i_L, to follow the desired reference envelope, i_r, as closely as possible. The best that can be achieved is to restrict the delay of i_L with respect to i_r to one switching period. To fulfill this goal, the following control law, which has been shown to give a good result, is chosen [8]:

$$i_r = i_L + T \frac{di_L}{dt} \tag{4.1}$$

where i_r is the current reference, i_L the current through the boost inductor, and T the switching period which is fixed by the desired switching frequency. Following this rule, di_L/dt is so adjusted that the error: $i_r - i_L$ will become zero in one switching period.

A complementary equation can be obtained by changing Eqn. (3.3) to the following form:

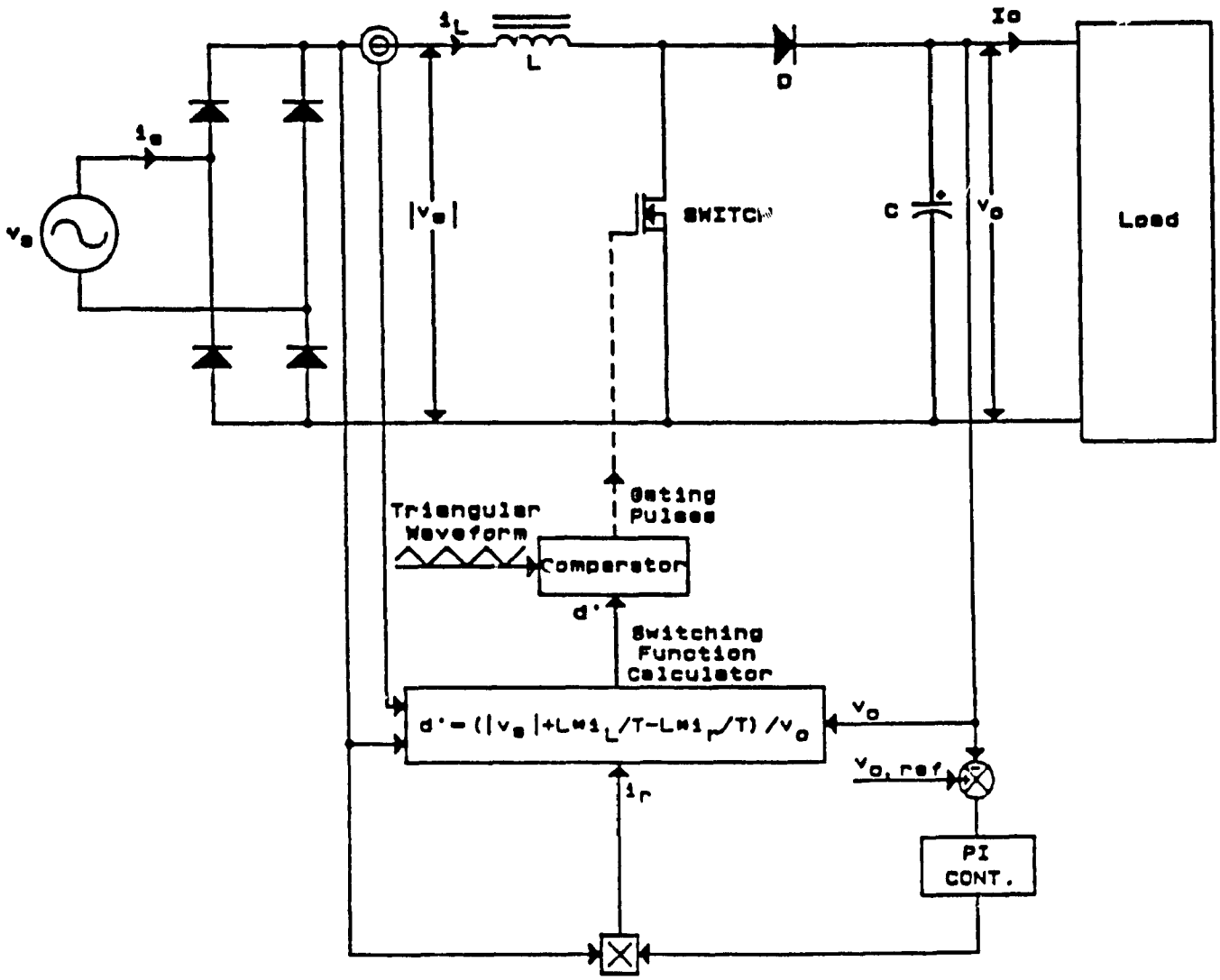

Fig. 4.1 A single-phase front-end diode-rectifier input current waveshaping circuit controlled using Method 1.

$$\frac{di_L}{dt} = \frac{|v_s| - d'v_o}{L} \tag{4.2}$$

where $|v_s|$ is the full-wave rectified AC input voltage, v_o the output voltage, and d' the average off-duty ratio of the switch over one switching period.

Combining Eqns. (4.1) and (4.2), results in

$$d' = \frac{1}{v_o}\left(|v_s| + \frac{L}{T} i_L - \frac{L}{T} i_r\right) \tag{4.3}$$

In order to produce the necessary gating pulses for the switch, d' should be compared with a triangular waveform of frequency equal to the desired switching frequency, and of maximum value equal to 1 and minimum value equal to 0 (based on the fact that d' can vary between 0 and 1).

The proposed computational method uses the signals of the input and output currents and voltages to calculate d' from which the gating signal for the switch is obtained. This method is well suited for a microprocessor-based implementation.

Since the inductor current follows the reference very closely, the low frequency error between i_L and i_r will be very small, resulting in very small low order harmonics in the input current.

The output voltage is kept constant through the voltage control loop shown in Fig. 4.1, by adjusting the amplitude of the current reference, the shape of which is determined by $|v_s|$.

Even though for very high switching frequencies, the T seconds delay of i_L with respect to i_r is negligible compared to the period of the line current, the above delay can be compensated by introducing a phase lead

equivalent to T seconds in the input voltage signal which is used as the template for the current. From the implementation point of view, it is not easy to phase shift a signal by a very small amount, since all-pass filters, which are normally used for this purpose, have limitations on the minimum possible amount of phase shift they can provide.

The feed forward of the load current signal to the output of the voltage controller can be further used to improve the transient behavior of the system.

4.2.2. Method 2

The second method is the simplified version of Method 1. The complexity of the control circuit is reduced by eliminating the need for input current sensing. This, however increases the sensitivity of the system to component value changes. Satisfactory performance is nevertheless shown to be maintained.

The basic circuit diagram of a single-phase front-end diode-rectifier followed by a step-up converter controlled by the second proposed control technique and used for the purpose of input current waveshaping, is shown in Fig. 4.2.

Eqn. (3.6) is repeated here for ease of reference:

$$d' = \frac{|v_s| - L\dfrac{di_L}{dt}}{v_o} \qquad (4.4)$$

Eqn. (4.4) can be changed to the following form, by introducing a factor P which is equal to 1 in the positive half cycle of v_s and -1 in the negative half cycle of v_s:

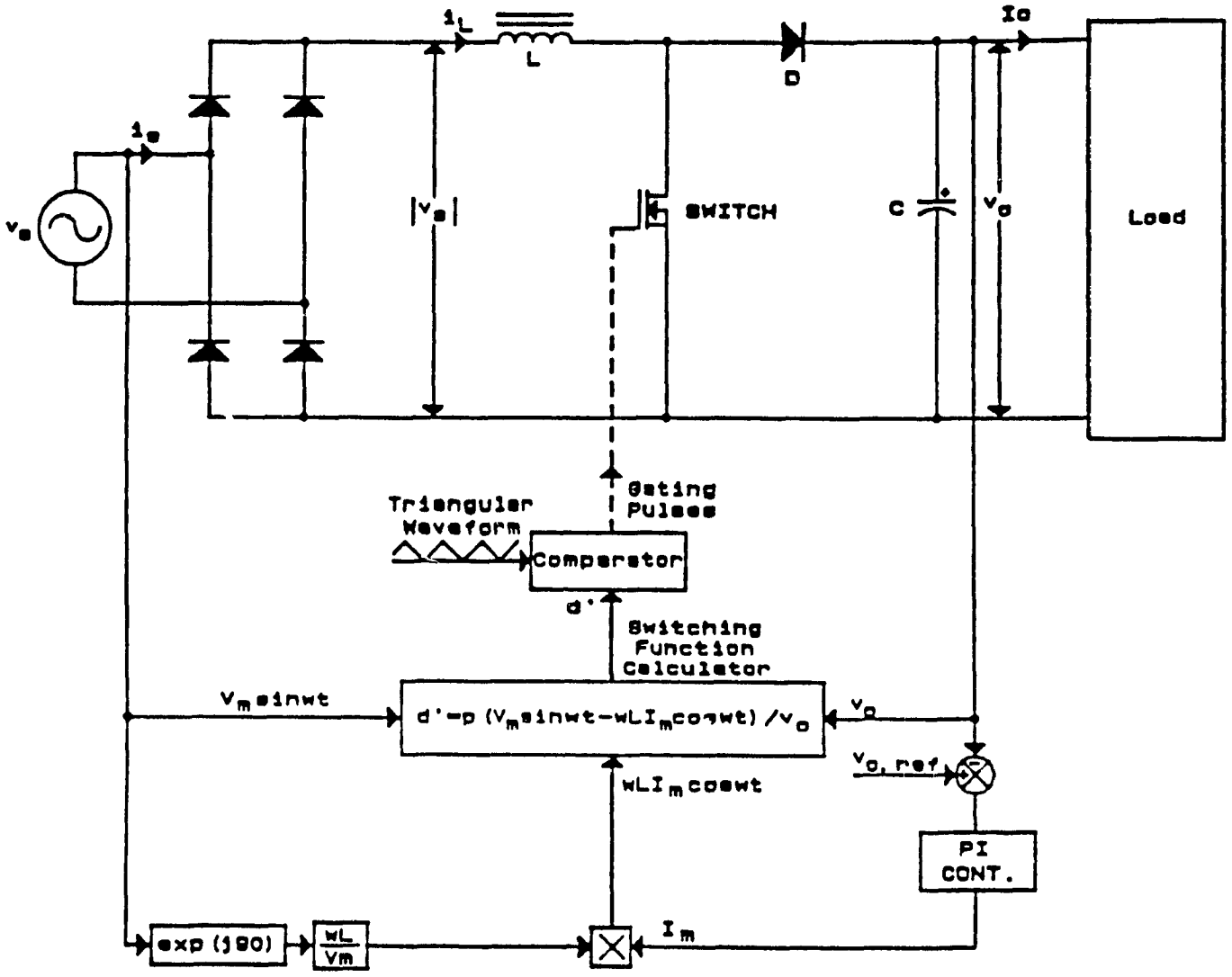

Fig. 4.2 A single-phase front-end diode-rectifier input current waveshaping circuit controlled using Method 2.

$$d' = P\,\frac{v_s - L\,\dfrac{di_s}{dt}}{v_o} \tag{4.5}$$

If the input current, i_s, were a perfect sine,

$$i_s = I_m \sin \omega t \tag{4.6}$$

then

$$\frac{di_s}{dt} = \omega I_m \cos \omega t \tag{4.7}$$

Therefore, the average off-duty ratio of the switch would vary according to the following relation:

$$d' = P\,\frac{V_m \sin \omega t - \omega L I_m \cos \omega t}{v_o} \tag{4.8}$$

In order to obtain a sinusoidal input current, the control circuit should compute d' according to Eqn. (4.8), triangulate it, and apply the resulting pulses to the boost switch. The amplitude of i_s (i.e., I_m) is dictated by the output voltage controller, while its shape is determined by v_s.

It is worth noting that since the current control system is open loop, the actual current may not follow exactly the reference . This will result in some distortion in the input current waveform in the form of low order harmonics.

The main advantage of the second control method is that it doesn't require any input current sensing.

4.3 Converter Analysis

Let us assume that the switching frequency is much higher than the line

frequency and the actual current waveform follows the current reference exactly (which can be realized to a very good approximation using one of the proposed computational control methods especially Method 1). Under these assumptions, whatever the design considerations discussed for the "Error Triangulation Method" in section 3.3, will also be valid for the two methods proposed in this chapter, since these two methods are also constant switching frequency techniques. ΔI (i.e., the peak-to-peak ripple current during one switching period), is given by Eqn. (3.4), and the variations of ΔI vs. time during a half cycle of the AC input voltage will be the same as that shown in Fig. 2.6, having performed the necessary modifications. $(\Delta I)_{ave}$ in a half cycle of the AC input voltage is given by Eqn. (3.5), and the variations of $(\Delta I)_{ave}$ vs. V_o and f_{sw} will be the same as those shown in Figs. (2.7) and (2.8) after performing the necessary modifications. Furthermore, the variations of the average on-duty ratio of the switch over one switching period is given by Eqn. (3.8).

4.4 Ratings of the Converter Components

The ratings will be the same as those found in section 2.4 .

4.5 Design Example

The design specifications and the base values are the same as those given in section 2.5, except for the desired switching frequency:

$$\text{Switching Frequency } (f_{sw}) = \text{constant} = 40 \text{ kHz.}$$

As in section 2.5,

$$i_s = 1 \text{ p.u.};$$

$$V_o = 1.91 \text{ p.u.};$$

and

$$R_L = 3.65 \text{ p.u.} .$$

The procedure for the design of L and C is exactly the same as that introduced in section 3.5, and the values for L and C will be the same as those found in that section.

4.6 Simulation Results

For the same reason as was mentioned in section 3.7, a ratio of switching frequency to line frequency lower than the one given in the design example is used for simulation purposes. The design specifications, the base values, and the component values are the same as those given in section 3.7.

Fig. 4.3 shows the simulation results for one complete cycle of the AC input voltage for Method 1. The frequency spectrum of the input current for Method 1 is shown in Fig. 4.4.

The input current THD is found to be 3.8% for Method 1. As seen, it is less than 5% and therefore no input filtering is required. The simulation results show that the input current is very close to sinusoidal and in phase with the AC input voltage; therefore, the input power factor is very close to 1 (0.9993 for the simulation performed).

Fig. 4.5 shows the simulation results for one complete cycle of the AC input voltage for Method 2. The frequency spectrum of the input current is shown in Fig. 4.6.

The input current THD is found to be 3.94% for Method 2. As expected, it is greater than the THD found for Method 1, but still less than 5%. There is no need for input filtering and the input current is seen to be very close to sinusoidal and in phase with the AC input voltage. The power factor is found

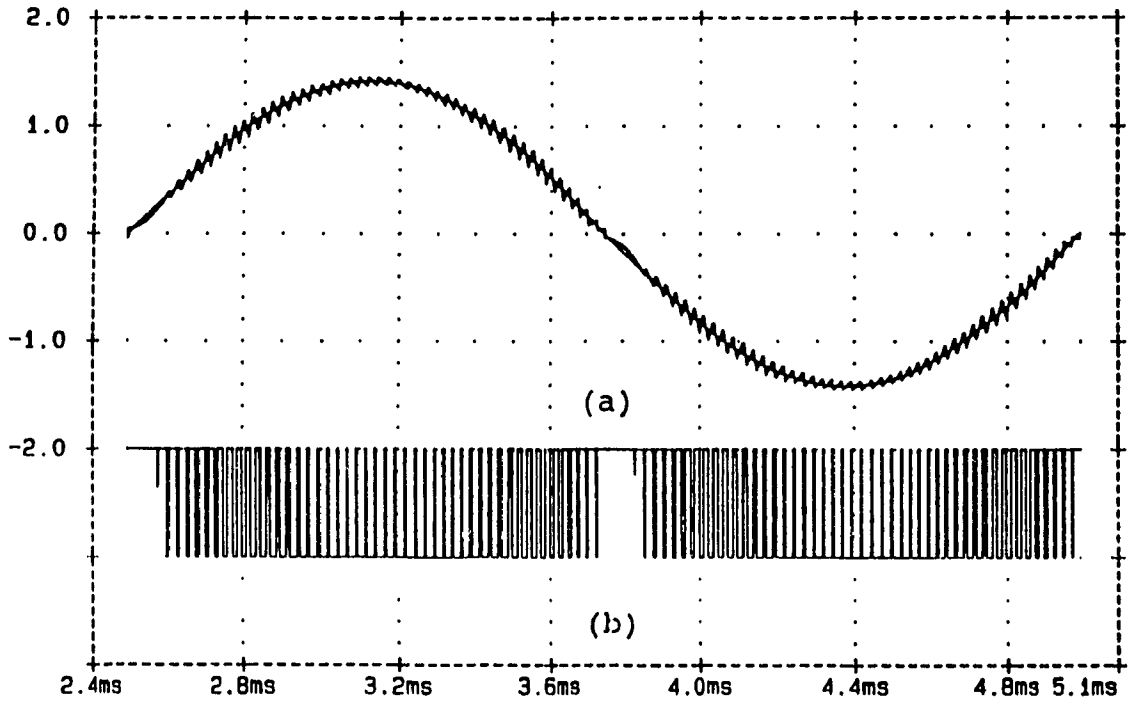

Fig. 4.3 Simulation results for one cycle of the AC input voltage (Method 1), (V_m = 1.414 p.u., V_o = 1.597 p.u., f_{line} = 1 p.u., I_m = 1.414 p.u., and L = 0.144 p.u.):

a) Line current and the current reference;

b) Gating signal of the switch.

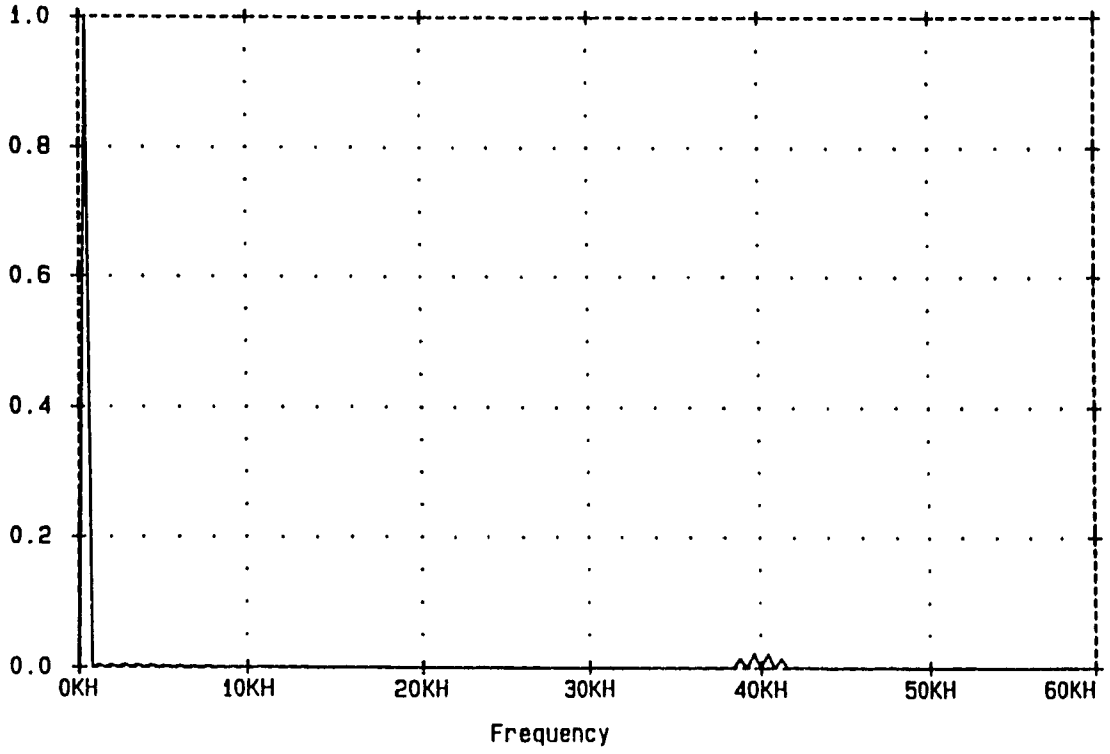

Fig. 4.4 Frequency spectrum of the input current (Method 1), (V_m = 1.414 p.u., V_o=1.597 p.u., f_{line}=1 p.u., I_m=1.414 p.u., and L=0.144 p.u.).

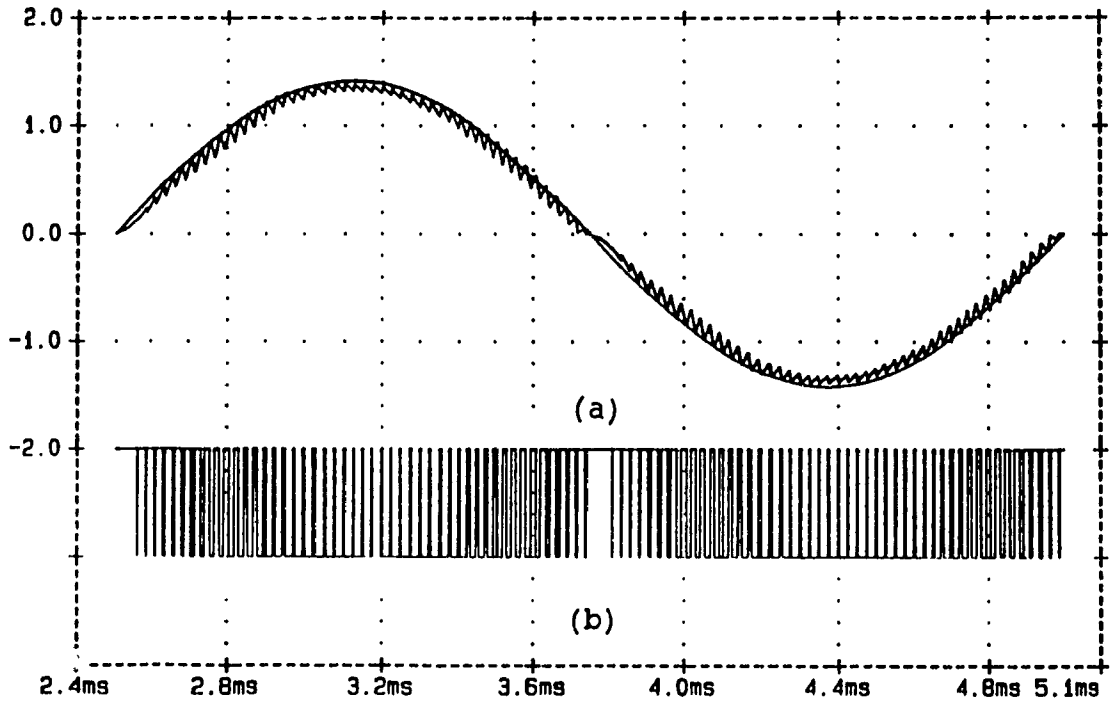

Fig. 4.5 Simulation results for one cycle of the AC input voltage (Method 2), (V_m= 1.414 p.u., V_o= 1.597 p.u., f_{line}= 1 p.u., I_m= 1.414 p.u., and L = 0.144 p.u.):

a) Line current and the current reference;

b) Gating signal of the switch.

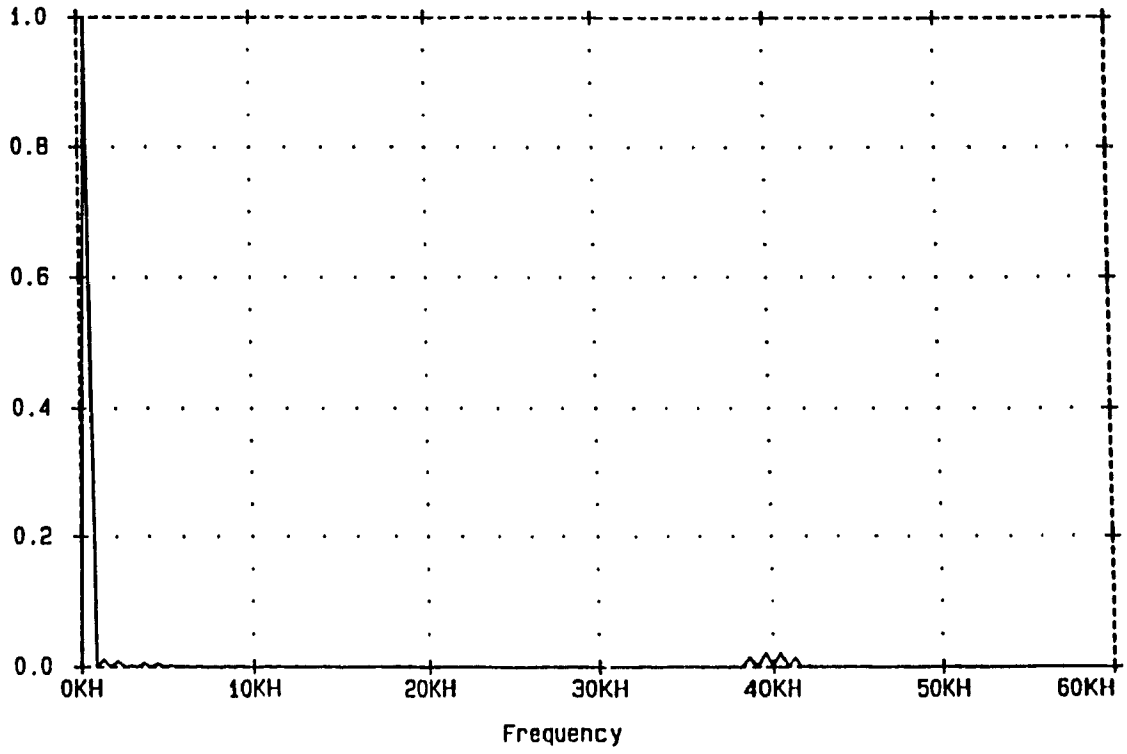

Fig. 4.6 Frequency spectrum of the input current (Method 2), (V_m = 1.414 p.u., V_o = 1.597 p.u., f_{line} = 1 p.u., I_m = 1.414 p.u., and L=0.144 p.u.).

to be 0.9992 for this case.

The sensitivity of the system to component value changes was checked by simulation. The performance is quite satisfactory for the component value changes in the order of 10% .

4.7 Experimental Results

A 1 kVA converter using the parameters given in the design example was set up in the laboratory. The waveforms of the input current and the AC input voltage obtained for both methods are shown in Figs. 4.7a and 4.8a, respectively. Also, the frequency spectrum of the input current for both control methods are shown in Figs. 4.7b and 4.8b, respectively.

The experimental results agree closely with the simulation results.

4.8 Conclusions

The predictive current waveshaping methods provide a lower distortion than the "Error Triangulation Method". They have the following main features:

- fixed switching frequency;
- instantaneous current control resulting in very fast response and switch reliability;
- controllable current ripple amplitude by choosing appropriate inductance value, and triangular waveform amplitude and frequency;
- no need for input current sensing with Method 2;
- no need for input filtering;
- suitability for microprocessor-based implementation.

However, the problem of system sensitivity to component value changes and tolerances always exists.

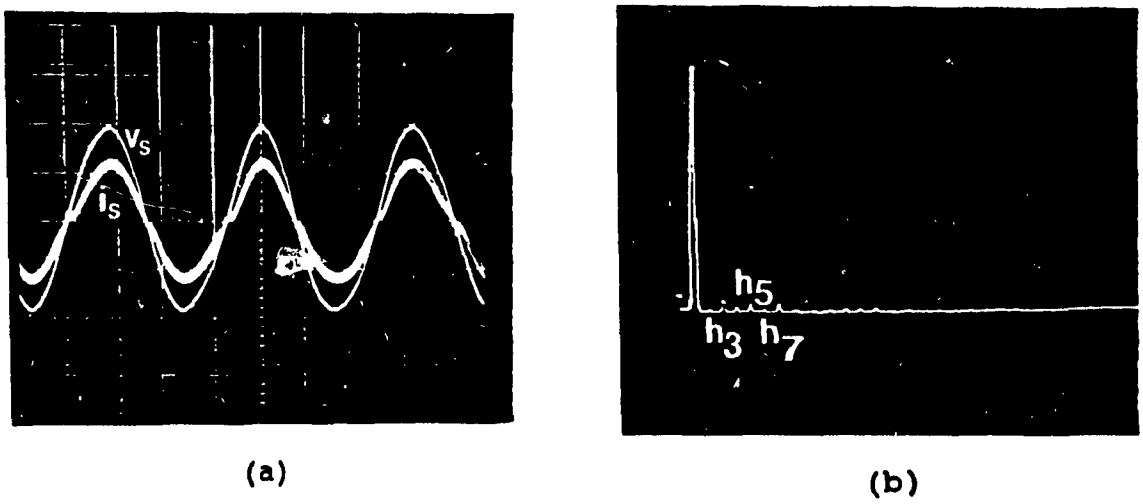

(a) (b)

Fig. 4.7 Experimental results (method 1):

a) Line current and input AC voltage waveforms (t=5 ms/div, current=10 A/div, voltage=84 v/div);

b) Line current harmonic spectrum.

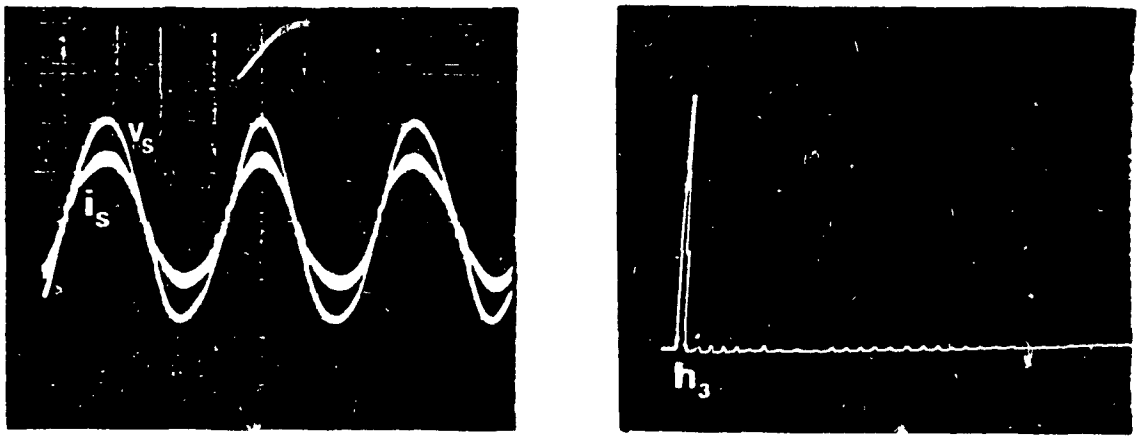

(a) (b)

Fig. 4.8 Experimental results (Method 2):

a) Line current and input AC voltage waveforms (t=5 ms/div, current=10 A/div, voltage=84 V/div);

b) Line current harmonic spectrum.

CHAPTER 5

COMPARATIVE EVALUATION

In this chapter, the bang-bang hysteresis technique (chapter 2) and the methods presented in chapters 3 and 4 will be compared with one another from different performance view points.

5.1 Switching Frequency

The frequency of switching is a very important issue in switched mode converters. A switching frequency out of the hearing frequency range is preferred to avoid audible noise. This defines the lower limit for the switching frequency. Also, the frequency can not be chosen to be very high, since high switching frequency means high switching losses, which is limited by switch technology and results in high stresses on switching devices and low efficiency. On the other hand, at high switching frequencies, the effect of Electromagnetic Interference (EMI) is significant and should be taken care of using EMI filters. However, as a rule, the higher the switching frequency, the smaller the size of the energy storage elements in the converter and also the closer the input current waveform to the ideal (reference) in input current waveshapers.

The foregoing discussion calls for a compromise in the choice of the frequency of switching. The medium power MOSFET switches available in the market can be operated at switching frequencies around 40 KHz with negligible

losses.

In constant switching frequency input current waveshaping techniques, the switching frequency can be fixed at the desired value, but in the techniques with free running operation, only the maximum or the average value of the switching frequency can be fixed. The "Error Triangulation Method" (chapter 3) and the predictive methods presented in chapter 4 are constant switching frequency techniques, while the hysteresis technique (chapter 2) results in varying switching frequency because of free running operation.

The constant switching frequency methods presented, provide a better switching pattern than the hysteresis technique, resulting in lower stresses on switching devices and higher switch reliability. Also, constant switching frequency techniques result in a far better frequency spectrum in the input current than the hysteresis method (with harmonics spread all over the frequency spectrum), making the task of input filtering (if required) easy and straight forward.

5.2 Converter Design

As was shown in the design example sections of chapters 2, 3, and 4, the design of the converter is much easier in the case of "Error Triangulation Method" and the predictive techniques presented than in the case of hysteresis technique. In hysteresis technique, imposing the condition of maximum allowed switching frequency and the condition for keeping the current within the hysteresis band, yield the appropriate value for L as well as ΔI (the hysteresis window size) using an iterative technique. Then, the specified maximum input current THD% should be used to design an input filter to take care of the THD% in excess of the specified value. In the constant

switching frequency techniques, on the contrary, the converter design is very straightforward; i.e., imposing the conditions of constant switching frequency and maximum allowed input current THD% at the same time, gives the appropriate value for L using a simple equation. The problem of input filtering almost does not exist, since proper choice of L results in the specified or less than the specified input current THD% (or ripple% in this special case).

5.3 Implementation

The hysteresis technique and the "Error Triangulation Method" are easily implementable using analog devices in the control circuit. The first predictive method presented in chapter 4 can also be implemented successfully using analog devices. This is due to the presence of the controlled current feedback which reflects the component and parameter changes and tolerances in the power and control circuits, resulting in appropriate counter measures from the control unit. The second predictive method presented in chapter 4, eliminates the need for current feedback, but is more sensitive to component and parameter value changes and tolerances.

Both predictive methods presented in chapter 4, are microprocessor implementable. Implementing a microprocessor-based control system can improve the performance of the system particularly with the second predictive method, by eliminating the problems like drift and component value changes associated with the analog devices.

However, working with the predictive methods always requires careful consideration of component value accuracy and adjustments, unless the technique used incorporates adaptive features.

5.4 Speed of Response

Even though all the techniques discussed in chapters 2, 3, and 4 are very fast current control methods, there is a slight difference between them from the point of view of speed of response to changes in the current level dictated by the output voltage controller.

Generally, predictive methods are known to be slower than the conventional current control techniques. This is particularly true in the predictive methods that do not use feedback of the controlled parameter, e.g., the inductor current in the case of input current waveshaping circuits. In such a case, the control circuit computes the duty cycle of the switch on the basis of estimated parameter values. Then if a change in the current is asked for, the duty cycle of the switch will be calculated according to the new value of the controlled parameter; but the appropriate initial condition for the after change period will not be established. In the conventional current mode control techniques and the predictive methods that use a feedback from the controlled current, on the contrary, a proper initial current value will be set up in the inductor for the instant following the change, and at the same time the duty cycle dictated to the switch by the control unit will be adjusted according to the new desired current level. This makes the predictive methods, not depending on the controlled current feedback, slower than the techniques using the feedback of the current. Sometimes, computational time is also added to the delay involved in the predictive methods.

Among the methods discussed in chapters 2, 3, and 4, the hysteresis technique, the "Error Triangulation Method" with P-controller and the first

predictive method presented in chapter 4, have almost the same speed of response and can be called instantaneous current control methods, while the "Error Triangulation Method" with PI-controller and the second predictive method presented in chapter 4 are characterized by a lower speed of response. The speed of response in the "Error Triangulation Method" with PI-controller is lowered as a result of introducing the integral term in the current controller. Simulation shows that for a 0.5 p.u. increase in the current reference, (under the same conditions that the simulation results of chapter 3 were obtained), the response time for the PI-controller option is in the order of 10 switching periods.

5.5 Size and Weight of the Power Circuit

The difference in the size and weight of the power processing stages of the input current waveshapers controlled by the techniques discussed in chapters 2, 3, and 4, is in the boost inductor and the input filter, since other parts of the power circuit do not change from one technique to another.

Under similar operating conditions, L was found (in the design example sections of chapters 2, 3, and 4)for the hysteresis and the constant switching frequency techniques to be

$$L_{hysteresis} = 0.04 \text{ p.u.};$$

and

$$L_{constant\ sw.\ freq.} = 0.026 \text{ p.u.} .$$

This means that a larger inductor is needed in the case of hysteresis control. The inductance value found for the constant switching frequency techniques is enough to limit the THD% (or ripple%) in the input current to

the permitted level, while the L found for the hysteresis method is not enough for the above purpose. In fact, to take care of the THD% in excess of the specified value, an input filter should be used adding to the size and weight of the converter.

5.6 Conclusions

It follows from the foregoing discussion that:

- Constant switching frequency techniques ("Error Triangulation Method" and the two predictive methods presented), result in a far better switching pattern than the hysteresis technique, lowering the stresses on the switching devices as well as making the task of input filtering easier.
- Design of L is easier in constant switching frequency methods than in the hysteresis technique. Also, choosing an appropriate L value limits the input current THD% (or ripple%) to the specified level.
- Implementation of the predictive methods presented, especially the one without the current feedback needs careful considerations. Both predictive methods presented are microprocessor-implementable.
- The hysteresis technique, the "Error Triangulation Method" with P-controller, and the first predictive method presented in chapter 4, have higher speed of response than the "Error Triangulation Method" with PI-controller and the second predictive method presented in chapter 4.
- Constant switching frequency techniques result in a considerable reduction in the size and weight of the passive components of the converter in comparison with the hysteresis technique.

CHAPTER 6

SUMMARY, CONCLUSIONS, AND SUGGESTIONS FOR FUTURE WORK

In this chapter, first, the contents of the previous chapters will be summarized briefly; then, some overall conclusions will be drawn; and finally, a few suggestions for future work will be given.

6.1 Summary

Chapter 1 gives an introduction to the issue of input power factor correction of front-end diode rectifier circuits through active input current waveshaping. The previous work done in the same area is reviewed and the scope of the work presented in the thesis is explained.

Chapter 2 explains the principles of operation and design aspects of the bang-bang hysteresis technique, i.e., the most widely used current control method for input current waveshaping of the front-end diode rectifiers. Also, some useful relations among the different parameters involved in the design of the converter controlled by the hysteresis technique are derived and the ratings of the components in the power circuit are obtained. Furthermore, design procedures are explained by an example, and simulation results are obtained to verify the theoretical concepts. Finally, the advantages and disadvantages of the hysteresis current control technique are listed.

Chapter 3 presents a new and effective current waveshaping technique with constant switching frequency, named "Error Triangulation Method". The

principles of operation and the design aspects of the above method are explained and the design procedures are given by an example. Also, the effects of using a PI-controller instead of a simple P-controller on the improvement of the current waveform are discussed. Furthermore, the output voltage to control input transfer function is derived and used in the design of the output voltage control loop. Finally, the theoretical concepts are verified by simulation and experimental results and some conclusions are made based on the characteristics of the "Error Triangulation Method".

Chapter 4 presents two constant switching frequency predictive current control techniques. The principles of operation and design aspects are explained and a sample converter controlled by the above methods is designed. Also, the problems with the predictive methods, especially those which do not use the feedback of current, from parameter sensitivity point of view are put forth. Furthermore, simulation and experimental results are used to verify the theoretical concepts. Finally, advantages and disadvantages of the predictive methods presented are listed.

Finally, chapter 5 compares the current control methods explained in chapters 2, 3, and 4 from different points of view.

6.2 Conclusions

Based on the characteristics of the methods discussed in chapters 2, 3, and 4, and the comparative evaluation performed in chapter 5, the following conclusions can be drawn:

- The switching patterns generated by constant switching frequency techniques (chapters 3 and 4) are much better than those created by the free-running methods (chapter 2). The stresses on the switching devices

are less and input filtering is easier in the constant switching frequency methods.

- Power circuit design is easier in the constant switching frequency techniques than in the free-running methods.
- The size and weight of the power circuit is reduced in the case of constant switching frequency techniques.
- The input current ripple% (or THD%) is controllable by proper design of the power circuit in the case of constant switching frequency methods.
- Predictive methods not using the input current feedback are both more parameter sensitive and slower in response than the methods using the current feedback.
- Predictive methods are microprocessor implementable.

6.3 Suggestions for Future Work

The current control techniques presented in chapters 3 and 4 are general purpose methods and can be used wherever current control is needed.

All the methods presented in this thesis are applicable to three-phase front-end diode rectifiers, even though only single-phase applications have been considered. For three-phase applications, three single-phase input current waveshaping units can be used, each being responsible for shaping the current in one of the phases, according to the corresponding voltage waveform. Three-phase applications of the methods presented are a possible extension of this work.

The predictive methods, presented in chapter 4, have been implemented using analog devices. Microprocessor-based implementation can lead to better results especially in the case of the second predictive method.

The "Error Triangulation Method" and the first predictive technique discussed in chapter 4, can be used to control the three-phase inverter in a current-controlled AC/AC frequency changer. Furthermore, a three-phase controlled rectifier with regeneration capability can be realized using the "Error Triangulation Method". Such a rectifier circuit, using the first predictive technique, has already been presented [8].

REFERENCES

[1] Ned Mohan, "Power Electronics: Converters, Applications, and Design", *John Willey & Sons*, 1989.

[2] Power Electronics Group, California Institute of Technology, "Input Current Shaped AC to DC Converters", *Final Report Prepared for NASA*, 1986.

[3] D. Gauger et al., "A Three-Phase Off-Line Switching Power Supply with Unity Power Factor and Low TIF", *IEEE American Power Electronics Conf. Rec.*, pp.115-121, March 1986.

[4] C. P. Henze and N. Mohan, "A Digitally Controlled AC to DC Power Conditioner that Draws Sinusoidal Input Current", *IEEE PESC '86 Conf. Rec.*, pp.531-540, June 1986.

[5] K. K. Sen and A. E. Emanuel, "Unity Power Factor Single-Phase Power Conditioner", *IEEE PESC '87 Conf. Rec.*, pp.516-524, June 1987.

[6] S. Manias and P. D. Ziogas, "An SMR Topology with Suppressed DC link Components and Predictive Line Current Waveshaping", *IEEE Trans. on Industry Applications*, Vol.IA-23, No. 4, pp.644-653, July-August 1987.

[7] M. F. Schlecht and B. A. Miwa, "Active Power Factor Correction for Switching Power Supplies", *IEEE Trans. on Power Electronics*, Vol. PE-2, No. 4, pp.273-281, October 1987.

[8] R. Wu, S. B. Dewan, and G. R. Slemon, "A PWM AC to DC Converter with Fixed Switching Frequency", *IEEE Ind. Appl. Soc. Ann. Meeting Conf. Rec.*, pp.706-711, Oct. 1988.

[9] O. Stihi and B. T. Ooi, "A Single-Phase Controlled-Current PWM

Rectifier", *IEEE Trans. on Power Electronics*, vol. 3, No. 4, pp.453-459, October 1988.

[10] J. H. Mulkern and N. Mohan, "A Sinusoidal Line Current Rectifier using zero-voltage Switching Step-up Converters", *IEEE Ind. Appl. Soc. Annual Meeting Conf. Rec.*, pp.767-771, 1988.

[11] A. R. Prasad, P. D. Ziogas, and S. Manias, "An Active Power Factor correction Technique for Three-Phase Diode Rectifiers", *IEEE PESC '89 Conf. Rec.*, pp.58-66, 1989.

[12] K. H. Liu and Y. L. Lin, "Current Waveform Distortion in Power Factor Correction Circuits Employing Discontinuous-Mode Boost Converters", *IEEE PESC '89 Conf. Rec.*, pp.825-829, 1989.

[13] M. Kazerani, G. Joos, and P. D. Ziogas, "A Novel Active Current Waveshaping Technique for Solid State Input Power Factor Conditioners", *IECON '89 Conf. Rec.*, Vol. 1, pp.99-105, Nov. 1989.

[14] M. Kazerani, G. Joos, P. D. Ziogas, "Programmable Input Power Factor Correction Methods for Single-Phase Diode-Rectifier Circuits", *APEC '90 Conf. Rec.*, March 1990.

[15] A. R. Prasad, P. D. Ziogas, and S. Manias, "A Comparative Evaluation of SMR Converters with and without Input Current Waveshaping", *IEEE Trans. on Industrial Electronics*, vol.35, No. 3, pp.461-468, August 1988.

[16] R. Redl and N. O. Sokal, "Current-Mode Control, Five Different Types, Used with the Three Basic Classes of Power Converters: Small-Signal AC and Large-Signal DC Characterization, Stability Requirements, and Implementation of Practical Circuits", *PESC '85 Conf. Rec.*, pp.771-785, June 1985.

[17] T. Kato and K. Miyao, "Modified Hysteresis control with Minor Loops for

Single-Phase Full-Bridge Inverters", *IEEE Ind. Appl. Soc. Annual Meeting Conf.Rec.*, vol. 1, pp.689-693, oct.1988.

[18] D. Di Cesare and M. Gambarara, "Boost LC^3 at Variable Constant", *Proc. Fourth ESTEC Spacecraft Power Conditioning Seminar (ESA Publication SP-186)*, pp.87-90, 1982.

[19] H. Le-Huy and L. A. Dessaint, "An Adaptive current Control Scheme for PWM Synchronous Motor Drives: Analysis and Simulation", *IEEE Trans on Power Electronics*, Vol. 4, No. 4, pp.486-495, Oct. 1989.

[20] M. Albach, "Conducted Interference Voltage of AC-DC Converters", *IEEE PESC '86 Conf. Rec.*, pp.203-212, 1986.

[21] L. Moran, P. D. Ziogas, and G. Joos, "Analysis and Design of a Three-Phase current Source Solid-State VAR Compensator, *IEEE PESC '87 Conf. Rec.*, 463-472, 1987.